



Modelling normal and nephrotic axial uptake of albumin and other filtered proteins along the proximal tubule

Aur lie Edwards¹ , Kimberly R. Long², Catherine J. Baty², Katherine E. Shipman²  and Ora A. Weisz² 

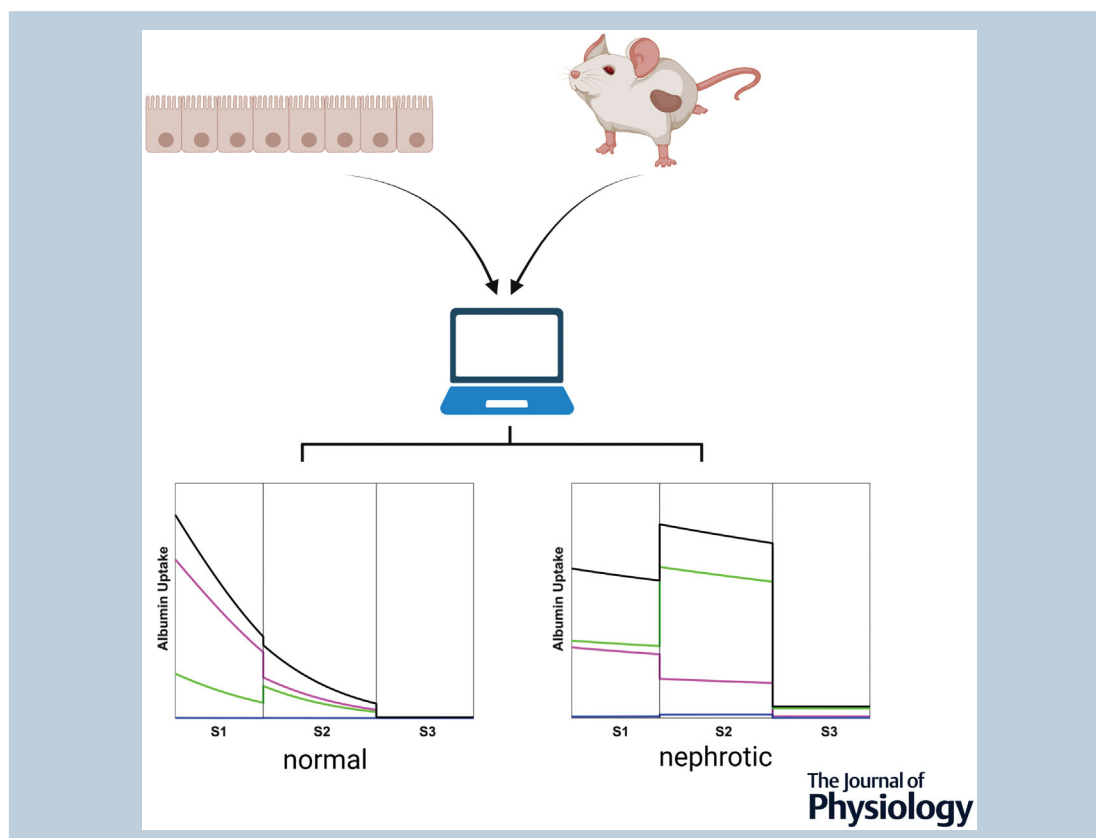
¹Department of Biomedical Engineering, Boston University, Boston, MA, USA

²Renal-Electrolyte Division, Department of Medicine, University of Pittsburgh School of Medicine, Pittsburgh, PA, USA

Edited by: Peking Fong & Helle Praetorius

Linked articles: This article is highlighted in a Translational Perspective article by Weinstein. To read this article, visit <https://doi.org/10.1113/JP282967>.

The peer review history is available in the Supporting Information section of this article (<https://doi.org/10.1113/JP282885#support-information-section>).



Aur lie Edwards is a Research Professor in Biomedical Engineering at Boston University. Her research focuses on solute transport mechanisms and regulation in the kidney. Current areas of interest include lifecycle adaptations in renal transporter profiles to maintain homeostasis, and the mechanisms underlying proteinuria.



Abstract Recent studies indicate that filtered albumin is retrieved in the proximal tubule (PT) via three pathways: receptor-mediated endocytosis via cubilin (high affinity) and megalin (low affinity), and fluid-phase uptake. Expression of megalin is required to maintain all three pathways, making it challenging to determine their respective contributions. Moreover, uptake of filtered molecules varies between the sub-segments (S1, S2 and S3) that make up the PT. Here we used new and published data to develop a mathematical model that predicts the rates of albumin uptake in mouse PT sub-segments in normal and nephrotic states, and partially accounts for competition by β_2 -microglobulin (β_2m) and immunoglobulin G (IgG). Our simulations indicate that receptor-mediated, rather than fluid-phase, uptake accounts for the vast majority of ligand recovery. Our model predicts that $\sim 75\%$ of normally filtered albumin is reabsorbed via cubilin; however, megalin-mediated uptake predominates under nephrotic conditions. Our results also suggest that $\sim 80\%$ of albumin is normally recovered in S1, whereas nephrotic conditions or knockout of cubilin shifts the bulk of albumin uptake to S2. The model predicts β_2m and IgG axial recovery profiles qualitatively similar to those of albumin under normal conditions. In contrast with albumin, however, the bulk of IgG and β_2m uptake still occurs in S1 under nephrotic conditions. Overall, our model provides a kinetic rationale for why tubular proteinuria can occur even though a large excess in potential PT uptake capacity exists, and suggests testable predictions to expand our understanding of the recovery profile of filtered proteins along the PT.

(Received 21 January 2022; accepted after revision 10 February 2022; first published online 17 February 2022)

Corresponding author A. Edwards: Department of Biomedical Engineering, Boston University, 44 Cummington Mall, Boston, MA 02215, USA. Email: aued@bu.edu

Abstract figure legend Data from mouse models and from cultured proximal tubule (PT) cells were used to create a mathematical model that predicts the uptake profile of albumin and other filtered ligands along the mouse PT in normal and nephrotic states. The distinct contributions of cubilin receptors (magenta), megalin receptors (green) and fluid phase uptake (blue) to total albumin retrieval (black) in S1, S2 and S3 sub-segments of the PT are delineated. Under normal conditions, albumin is primarily recovered in the S1 sub-segment by cubilin, whereas under nephrotic conditions the majority is retrieved in S2. Other proteins exhibit strikingly different uptake profiles. Our model explains how the distribution and capacity of high-affinity and low-affinity uptake pathways enable uptake of albumin over a broad range of filtered concentrations, and how tubular proteinuria can occur despite a large excess in potential PT uptake capacity. Created with BioRender.com

Key points

- We used new and published data to develop a mathematical model that predicts the profile of albumin uptake in the mouse proximal tubule in normal and nephrotic states, and partially accounts for competitive inhibition of uptake by normally filtered and pathological ligands.
- Three pathways, consisting of high-affinity uptake by cubilin receptors, low-affinity uptake by megalin receptors and fluid phase uptake, contribute to the overall retrieval of filtered proteins.
- The axial profile and efficiency of protein uptake depend on the initial filtrate composition and the individual protein affinities for megalin and cubilin.
- Under normal conditions, the majority of albumin is retrieved in sub-segment S1 but shifts to sub-segment S2 under nephrotic conditions. Other proteins exhibit different uptake profiles.
- Our model explains how tubular proteinuria can occur despite a large excess in potential proximal tubule uptake capacity.

Introduction

A primary function of the kidney proximal tubule (PT) is to recover albumin and other plasma proteins that escape the glomerular filtration barrier. Under normal conditions, the barrier presents a formidable obstacle that

limits protein entry into the tubule lumen, and proteins are retrieved nearly completely to maintain a protein-free urine. In disease conditions where the glomerular barrier is impaired, considerably higher concentrations of plasma proteins enter the tubule. Recent studies demonstrate that

under these conditions, the PT exhibits a large reserve capacity for recovering filtered proteins that is orders of magnitude above the normal level (Weyer *et al.* 2018).

The efficient retrieval of filtered proteins is mediated by megalin and CUBAM (comprising cubilin and amnionless (AMN) subunits) receptors that are abundantly expressed in PT cells (Christensen *et al.* 2012a; Eshbach & Weisz, 2017). Megalin and CUBAM are known to associate in a complex but can also function independently to retrieve ligands. The cytoplasmic domains of megalin and AMN mediate clathrin-dependent endocytosis by binding to the clathrin adaptor protein disabled-2 (Dab2). After internalization, ligands are dissociated from their receptors in apical endosomes and targeted for degradation, while receptors are recycled back to the apical surface (Christensen *et al.* 2012a; Eshbach & Weisz, 2017).

Studies using knockout (KO) mice and siRNA in cell culture have begun to elucidate the pathways involved in endocytic retrieval of filtered proteins, as well as the selective roles of megalin and cubilin in these processes (Weisz, 2021). Deconvolution of albumin uptake curves in a highly differentiated opossum kidney (OK) cell culture model of the PT revealed three components: a high-affinity component of $K_m \sim 50 \mu\text{g ml}^{-1}$, a low-affinity component of $K_m \sim 300 \mu\text{g ml}^{-1}$, and a non-saturable component (Ren *et al.* 2020). No clathrin-independent apical uptake pathways have been described in PT cells, and the non-saturable component is assumed to represent uptake in the fluid incorporated into clathrin-coated vesicles. Knockdown of cubilin reduced the capacity of the high affinity component whereas depletion of megalin obliterated the low affinity component, suggesting that these receptors mediate high- and low-affinity uptake of albumin, respectively. While fluid-phase uptake is negligible at low concentrations of albumin, it represents a significant contribution to albumin recovery by OK cells at very high concentrations (Ren *et al.* 2020).

The availability of three uptake pathways with distinct affinities and capacities provides the flexibility to efficiently retrieve filtered albumin using a saturable, receptor-mediated pathway tailored to normally filtered concentrations of ligand, while also maintaining reserve capacity to accommodate the increases in albumin filtration that occur in nephrotic disease. Indeed, studies in KO mice confirm that the PT maintains a very high reserve capacity to take up protein under nephrotic conditions (Weyer *et al.* 2018). Much of this reserve capacity is directly dependent on the expression of megalin and CUBAM receptors, as knockout of megalin and cubilin in podocin-deficient mice increased urinary excretion of albumin by 40% over podocin alone (Weyer *et al.* 2018). The demonstration of very high retrieval of albumin in microdissected perfused rabbit tubules attributed to fluid-phase endocytosis

suggests the possibility that this mechanism of uptake may contribute significantly to albumin recovery under nephrotic conditions (Park & Maack, 1984).

Understanding the contribution of each uptake pathway to the recovery of normal and nephrotic levels of albumin is complicated by axial heterogeneity along the PT. The PT is divided into three sub-segments, termed S1, S2 and S3, that differ both morphologically and functionally (Zhai *et al.* 2003; Kalakeche *et al.* 2011; Christensen *et al.* 2012b; Lee *et al.* 2015; Limbutara *et al.* 2020). Expression of megalin and cubilin receptors, endocytic pathway markers and Dab2 varies between sub-segments (Schuh *et al.* 2018; Limbutara *et al.* 2020; Christensen *et al.* 2021). The relative contribution of each albumin uptake pathway within a given sub-segment will depend in part on the level of receptor expressed and the concentration of ligand along the PT axis. Under nephrotic conditions where tubular albumin levels exceed the saturable capacity, fluid reabsorption along the tubule axis will progressively increase the luminal albumin concentration, potentially enhancing the contribution of fluid-phase uptake to overall albumin retrieval in more distal PT sub-segments.

Adding to the challenge of deciphering the contribution of each receptor/uptake pathway on albumin retrieval is that all three uptake pathways are reliant on the expression of megalin and Dab2. Loss of megalin or Dab2 expression in vertebrates leads to a dramatic reduction in the number of apical endocytic compartments, including endocytic vesicles (Nagai *et al.* 2005; Kur *et al.* 2011; Dachy *et al.* 2015). As a consequence, trafficking of CUBAM is impaired, and uptake via fluid-phase is also considerably reduced in either megalin or Dab2 KO cells (Ren *et al.* 2020).

In the present study, we used published and new experimental data to create a model that describes the axial uptake of filtered albumin in normal and nephrotic states in mice. Our model accounts partially for the potential competition for receptor-mediated uptake of filtered proteins other than albumin whose relative tubular concentrations varies based on glomerular barrier integrity, and compares their uptake to that of albumin. Endocytic responses to changes in flow that have been documented in cell culture are also included (Raghavan *et al.* 2014; Long *et al.* 2017).

Methods

Experimental protocols

Ethical approval. All experimental procedures were approved by the Institutional Animal Care and Use Committee of the University of Pittsburgh (IACUC approval no. 21079537).

Axial uptake of dextran in mouse PT. C57/BL6 mice (2 males and 2 females, 10 weeks) were injected intracardially with 0.75 mg 10 kD Alexa FluorTM 568 dextran (Thermo Fisher Scientific, Waltham, MA, USA, cat. no. D22912) and sacrificed after 3 min (using isoflurane). Kidneys were harvested and immediately sectioned. Dextran was visualized in living kidney sections (2 mice). The remaining kidney was fixed and sectioned, and stained with antibodies to highlight PT segments (S1: SGLT2, Abcam, Cambridge, MA, USA, cat. no. 85626, 1:400; S2: OAT1, Alpha Diagnostic, San Antonio, TX, USA, cat. no. OAT11A, 1:200; S3: aquaporin-4, Alomone Labs, Jerusalem, Israel, cat. no. AQP-004, 1:500). Images were obtained using a Leica SP8 inverted confocal microscope (Leica Microsystems, Buffalo Grove, IL, USA) with environmental chamber, motorized stage, and $\times 25$, 0.95 numerical aperture (NA) and $\times 40$, 1.1 NA water objectives. Tilesans were generated to document important anatomic landmarks to facilitate interpretation of PT segments. Dextran uptake was grossly quantitated from line profiles drawn perpendicular to the PT segment using LASX software from maximum projections of the live dataset (3 tilesans from one male). Approximately 45 line scans contributed to mean intensity estimate for presumed S2 and 10 line scans for confirmed S1 as it was observed to emerge from glomerulus.

Impact of IgG and β_2 -microglobulin on albumin uptake. Opossum kidney cells (RRID:CVCL_0472; OK-P subclone originally obtained from M. Levi, Georgetown University) were cultured on transwell supports under continuous orbital shear stress as described in Long *et al.* (2017). Cells grown in this manner harbour key features of PT cells *in vivo*, including a highly developed brush border and apical endocytic pathway, and high levels of megalin, cubilin and Dab2 expression (Long *et al.* 2017; Park *et al.* 2020; Ren *et al.* 2020). Alexa Fluor-647 goat anti-rabbit immunoglobulin G (IgG) was purchased from Invitrogen (cat. no. A21245). Native human β_2 -microglobulin (β_2m) was purchased from Bio-Rad Laboratories, Hercules, CA, USA (cat. no. 0824) and conjugated to Alexa Fluor-647 using the Alexa FluorTM 647 Protein Labelling Kit (Thermo Fisher Scientific, cat. no. A20173). To assess whether these ligands compete for albumin uptake and vice versa, OK cells were incubated in serum-free medium with the indicated concentrations of Alexa Fluor-488 albumin (Thermo Fisher Scientific, cat. no. A13100) and either Alexa Fluor-647 IgG or β_2m for 15 min at 37°C, then solubilized and cell-associated fluorescence quantified by spectrofluorimetry as described (Long *et al.* 2017; Ren *et al.* 2020). Control studies confirmed that there was no appreciable bleed-through between the emission wavelengths used to quantify each ligand.

Uptake of IgG and β_2m by PT cells. To measure concentration-dependent uptake of IgG and β_2m by PT cells, OK cells were incubated with increasing concentrations of each ligand as above. The contribution of fluid-phase uptake was determined in parallel samples by the inclusion of 2 g l⁻¹ unlabelled fatty-acid free albumin (Sigma, St Louis, MO, USA, cat. no. A7030) to compete for receptor-mediated uptake. Studies in CRISPR/Cas9 *Cubn* KO *versus* control cells were performed to determine the role of cubilin in uptake of both ligands (Long *et al.* 2022).

Model description

The present model describes the transport of albumin, β_2m and IgG in the PT. The tubule is represented as a rigid cylinder of fixed radius R and length L , with axial coordinate z . Cubilin-mediated endocytosis and megalin-mediated endocytosis are modelled as saturable processes that obey Michaelis–Menten kinetics, whereas fluid-phase uptake is proportional to the rate of fluid internalization and solute concentration.

Fluid flow profile. Fluid flow in the tubular lumen is taken to decrease exponentially (Weinstein *et al.* 2007). The local flow $Q(z)$ and local mean velocity $u(z)$ are then given by (Gliozzi *et al.* 2020; Edwards *et al.* 2021):

$$u(z) = \frac{Q(z)}{\pi R^2} = \frac{Q_0 \exp(-\omega z)}{\pi R^2} = u_0 \exp(-\omega z) \quad (1)$$

where Q_0 and u_0 denote the flow and velocity at the tubule entrance. The parameter ω , which governs the rate of change, is calculated knowing the fraction (f_w) of water that is reabsorbed over length L :

$$Q(L) = Q_0 \exp(-\omega L) = (1 - f_w) Q_0 \quad (2a)$$

$$\omega = -\frac{\ln(1 - f_w)}{L} \quad (2b)$$

Note that the model assumes variable rates of ion-driven (non-endocytotic) fluid reabsorption in S1–S2 *versus* S3, to account for possible segment-dependent variations in f_w in response to specific experimental manoeuvres or drugs.

Albumin concentration profile. In the following equations, C_{alb} denotes the luminal concentration of albumin, C_b the luminal concentration of β_2m and C_i the luminal concentration of IgG. Taking into account the three uptake pathways as well as potential competition

between filtered proteins, the flux of albumin at the apical surface J_{alb} is given by:

$$J_{\text{alb}}(z) = \frac{V_m^{\text{cub}}(z) (C_{\text{alb}}/K_{m,\text{alb}}^{\text{cub}})}{1 + (C_{\text{alb}}/K_{m,\text{alb}}^{\text{cub}}) + (C_b/K_{m,b}^{\text{cub}}) + (C_i/K_{m,i}^{\text{cub}})} + \frac{V_m^{\text{meg}}(z) (C_{\text{alb}}/K_{m,\text{alb}}^{\text{meg}})}{1 + (C_{\text{alb}}/K_{m,\text{alb}}^{\text{meg}}) + (C_b/K_{m,b}^{\text{meg}}) + (C_i/K_{m,i}^{\text{meg}})} + J_{v,\text{up}}(z) C_{\text{alb}} \quad (3)$$

The first and second terms respectively describe cubilin- and megalin-mediated uptake, and the third term fluid-phase uptake. $K_{m,\text{alb}}$ is the affinity of cubilin (superscript 'cub') or megalin (superscript 'meg') to albumin, $K_{m,b}$ is the affinity of cubilin or megalin to $\beta 2\text{m}$, $K_{m,i}$ is the affinity of cubilin or megalin to IgG, V_m is the maximum uptake capacity via cubilin or megalin at coordinate z , and $J_{v,\text{up}}$ is the rate of volume internalization via fluid-phase uptake. Assuming no binding of $\beta 2\text{m}$ or IgG to megalin (see below), Eqn (3) can be simplified as:

$$J_{\text{alb}}(z) = \frac{V_m^{\text{cub}}(z) C_{\text{alb}}}{C_{\text{alb}} + K_{m,\text{alb}}^{\text{cub}} (1 + C_b/K_{m,b}^{\text{cub}} + C_i/K_{m,i}^{\text{cub}})} + \frac{V_m^{\text{meg}}(z) C_{\text{alb}}}{C_{\text{alb}} + K_{m,\text{alb}}^{\text{meg}}} + J_{v,\text{up}}(z) C_{\text{alb}} \quad (4)$$

To account for the flow-dependence of endocytosis (Raghavan *et al.* 2014; Long *et al.* 2017), we assume that V_m varies as follows:

$$V_m(z) = V_{\text{max}} (0.5 + 0.5u(z)/u_0^*) \quad (5)$$

V_{max} represents the maximum uptake capacity; since it is proportional to receptor expression, its value differs between S1, S2 and S3. The parameter u_0^* denotes the entrance velocity under basal (normal) conditions.

Conservation of albumin at steady state can be written as (Gliozzi *et al.* 2020; Edwards *et al.* 2021):

$$\frac{d(uC_{\text{alb}})}{dz} = -\frac{2}{R} J_{\text{alb}}(z) \quad (6)$$

Equation (6) implicitly assumes that albumin transport is not limited by diffusion from the bulk fluid to the base of the microvilli. A previous model found that accounting for mass transfer resistance in the intermicrovillar space has only a modest effect (Lazzara & Deen, 2007), and comparing model predictions with/without diffusional resistance in a simple case here showed minimal impact on uptake (results not shown). Hence, as in more recent models (Gliozzi *et al.* 2020; Edwards *et al.* 2021), we omitted mass transfer resistance in favour of a

simpler approach. Combining Eqns (1), (4) and (6), we have:

$$u_0 \exp(-\omega z) \left(\frac{dC_{\text{alb}}}{dz} - \omega C_{\text{alb}} \right) = -\frac{2}{R} \left[\frac{V_m^{\text{cub}}(z) C_{\text{alb}}}{C_{\text{alb}} + K_{m,\text{alb}}^{\text{cub}} (1 + C_b/K_{m,b}^{\text{cub}} + C_i/K_{m,i}^{\text{cub}})} + \frac{V_m^{\text{meg}}(z) C_{\text{alb}}}{C_{\text{alb}} + K_{m,\text{alb}}^{\text{meg}}} + J_{v,\text{up}}(z) C_{\text{alb}} \right] \quad (7)$$

After taking into account Eqn. (5) and simplifying, we obtain:

$$\frac{dC_{\text{alb}}}{dz} = -\frac{2}{Ru_0 \exp(-\omega z)} \times \left[\left(\frac{V_{\text{max}}^{\text{cub}} C_{\text{alb}}}{C_{\text{alb}} + K_{m,\text{alb}}^{\text{cub}} (1 + C_b/K_{m,b}^{\text{cub}} + C_i/K_{m,i}^{\text{cub}})} + \frac{V_{\text{max}}^{\text{meg}} C_{\text{alb}}}{C_{\text{alb}} + K_{m,\text{alb}}^{\text{meg}}} \right) \times (0.5 + 0.5 \exp(-\omega z) u_0/u_0^*) + J_{v,\text{up}}(z) C_{\text{alb}} \right] + \omega C_{\text{alb}} \quad (8)$$

Similarly, the luminal concentrations of $\beta 2\text{m}$ and IgG respectively obey the following equations:

$$\frac{dC_b}{dz} = -\frac{2}{Ru_0 \exp(-\omega z)} \times \left[\left(\frac{V_{\text{max}}^{\text{cub}} C_b}{C_b + K_{m,b}^{\text{cub}} (1 + C_{\text{alb}}/K_{m,\text{alb}}^{\text{cub}} + C_i/K_{m,i}^{\text{cub}})} \right) \times (0.5 + 0.5 \exp(-\omega z) u_0/u_0^*) + J_{v,\text{up}}(z) C_b \right] + \omega C_b \quad (9)$$

$$\frac{dC_i}{dz} = -\frac{2}{Ru_0 \exp(-\omega z)} \times \left[\left(\frac{V_{\text{max}}^{\text{cub}} C_i}{C_i + K_{m,i}^{\text{cub}} (1 + C_{\text{alb}}/K_{m,\text{alb}}^{\text{cub}} + C_b/K_{m,b}^{\text{cub}})} \right) \times (0.5 + 0.5 \exp(-\omega z) u_0/u_0^*) + J_{v,\text{up}}(z) C_i \right] + \omega C_i \quad (10)$$

Equations (8–10) are solved using MATLAB (The MathWorks Inc., Natick, MA, USA), after specifying the entrance conditions $C_{\text{alb}}(z=0)$, $C_b(z=0)$ and $C_i(z=0)$, namely the concentrations of albumin, $\beta 2\text{m}$ and IgG in the glomerular filtrate. We consider both short (SLN) and long

Table 1. Parameter values – baseline

Parameter	Value	Reference
Functional tubule length, L	SLN: 5.12 mm (S1 1.51 mm, S2 1.94 mm, S3 1.67 mm) LLN: 6.17 mm (S1 2.41 mm, S2 1.88 mm, S3 1.88 mm)	Letts <i>et al.</i> (2017), Christensen <i>et al.</i> (2021) (see text)
Proximal tubule radius, R	10.8 μm	Letts <i>et al.</i> (2017)
Glomerular filtration rate, GFR	295 $\mu\text{l min}^{-1}$	Hashimoto <i>et al.</i> (2005)
Single nephron GFR, Q_0	11.7 nl min^{-1}	Hashimoto <i>et al.</i> (2005)
Reference fluid velocity at entrance, u_0^*	0.53 mm s^{-1}	
Fractional water reabsorption, f_w	60% (50% in S1–S2, 10% in S3)	Hashimoto <i>et al.</i> (2005)
Rate of flow decrease, ω	SLN: 0.201 mm^{-1} in S1–S2, 0.063 mm^{-1} in S3 LLN: 0.162 mm^{-1} in S1–S2, 0.056 mm^{-1} in S3	
Concentration of albumin in filtrate	30.5 nmol l^{-1} (2.0 mg l^{-1})	Weyer <i>et al.</i> (2018)
Concentration of $\beta 2\text{m}$ in filtrate	117.7 nmol l^{-1} (1.37 mg l^{-1})	See text
Concentration of IgG in filtrate	0.625 nmol l^{-1} (0.1 mg l^{-1})	See text
Affinity of cubilin to albumin, $K_{\text{m,alb}}^{\text{cub}}$	672 nmol l^{-1} (44 mg l^{-1})	Ren <i>et al.</i> (2020)
Affinity of cubilin to $\beta 2\text{m}$, $K_{\text{m,b}}^{\text{cub}}$	420 nmol l^{-1} (4.87 mg l^{-1})	Leheste <i>et al.</i> (1999)
Affinity of cubilin to IgG, $K_{\text{m,i}}^{\text{cub}}$	625 nmol l^{-1} (100 mg l^{-1})	See text
Affinity of megalin to albumin, $K_{\text{m,alb}}^{\text{meg}}$	4504 nmol l^{-1} (295 mg l^{-1})	Ren <i>et al.</i> (2020)
Relative density of cubilin	S1: 0.54, S2: 0.34, S3: 0.12	Limbutara <i>et al.</i> (2020)
Maximum uptake capacity via cubilin, $V_{\text{max}}^{\text{cub}}$	2.27 $\text{fmol s}^{-1} \text{mm}^{-2}$ S1: $2.27 \times 0.608 = 1.38$ S2: $2.27 \times 0.375 = 0.85$ S3: $2.27 \times 0.017 = 0.04$	Estimated
Relative density of megalin	S1: 0.24, S2: 0.49, S3: 0.27	Limbutara <i>et al.</i> (2020)
Maximum uptake capacity via megalin, $V_{\text{max}}^{\text{meg}}$	6.38 $\text{fmol s}^{-1} \text{mm}^{-2}$ S1: $6.38 \times 0.308 = 1.97$ S2: $6.38 \times 0.646 = 4.12$ S3: $6.38 \times 0.046 = 0.29$	Estimated
Rate of volume internalization via fluid-phase uptake, $J_{\text{v,up}}$	S1: 0.111 $\text{nl min}^{-1} \text{mm}^{-2}$ S2: 0.233 $\text{nl min}^{-1} \text{mm}^{-2}$ S3: 0.017 $\text{nl min}^{-1} \text{mm}^{-2}$	Gekle <i>et al.</i> (1995) See text

(LLN) loop nephrons, which are taken to differ only by the length of their sub-segments S1, S2 and S3. Hence, Eqns (8–10) are solved separately for SLN and LLN, and total uptake is computed based upon the SLN-to-LLN ratio in mice, taken as 64:36 (Ichii *et al.* 2006). The computational code is available from the corresponding author upon request.

Model parameters. Parameter values are summarized in Table 1. The total length of the PT was set to 5.1 mm in SLNs and 6.2 mm in LLNs (Letts *et al.* 2017). In the absence of mouse-specific data, we assumed that the relative lengths of S1, S2 and S3 in SLN and LLN are equal to those measured in the rat (Christensen *et al.* 2021). The analysis of anatomical data by Knepper and colleagues (Clark *et al.* 2019) suggests that rat and mouse have similar distributions of PT sub-segments, although their estimate of the relative abundance of S3 cells relative to S1 and S2 in both species is lower than that recently reported (Christensen *et al.* 2021).

The values of $V_{\text{max}}^{\text{cub}}$ and $V_{\text{max}}^{\text{meg}}$ in S1, S2 and S3 were taken to be proportional to the relative expression of cubilin and megalin in each segment. The latter was determined from the protein expression levels of cubilin and megalin determined by quantitative proteomics of rat nephron segments (Limbutara *et al.* 2020). Because the S3 segment contains a relatively undeveloped endocytic pathway relative to S1 and S2 (Christensen *et al.* 2012b, 2021) and also expresses dramatically reduced levels of Dab2 (~13% that of S1 or S2 cells) (Limbutara *et al.* 2020), we corrected megalin and cubilin V_{max} values to account for the presumed reduction in endocytic rate in this segment (Table 1). Specifically, the proteomic expression of cubilin in S1, S2 and S3 was reported as 679335, 419164 and 150646, respectively (Limbutara *et al.* 2020). After multiplying the value in S3 by 0.13, the fractional 'effective' cubilin expression was computed as 60.8% in S1, 37.5% in S2 and 1.7% in S3. Similarly, the proteomic expression of megalin in S1, S2 and S3 is 1526800, 3194703 and 1744919, respectively (Limbutara *et al.* 2020). With the

Dab2 correction in S3, the fractional 'effective' megalin expression was computed as 30.8% in S1, 64.6% in S2 and 4.6% in S3.

From the observation that static OK cells reabsorb 0.6% of their volume per minute (Gekle *et al.* 1995), we estimated the rate of volume internalization via fluid-phase uptake ($J_{v,up}$) in S1 as $0.111 \text{ nl min}^{-1} \text{ mm}^{-2}$, based on an average cell height of $18.5 \mu\text{m}$ (unpublished confocal imaging data). Assuming that fluid-phase uptake is proportional to megalin and Dab2 expression, $J_{v,up}$ was set to $0.111 \times 64.6/30.8 = 0.233 \text{ nl min}^{-1} \text{ mm}^{-2}$ in S2, and $0.111 \times 4.6/30.8 = 0.017 \text{ nl min}^{-1} \text{ mm}^{-2}$ in S3.

To our knowledge, the concentration of albumin in the glomerular filtrate has not been measured directly in mice. Estimates based upon albumin excretion in KO models range from 0.5 mg l^{-1} (Mori *et al.* 2017) to 4 mg l^{-1} (Weyer *et al.* 2011). We choose an intermediate value of 2.0 mg l^{-1} (30.5 nM), which is close to the value of 1.9 mg l^{-1} derived from the study of Weyer *et al.* (2018).

The filtrate concentration of IgG was determined as the product of plasma IgG concentration, for which we found values ranging from 2 to 6 mg ml^{-1} in mice (Mink &

Benner, 1979; Klein-Schneegans *et al.* 1989; Honjo *et al.* 2012), and the IgG sieving coefficient, which was reported as 1.4×10^{-5} in mouse and 4.2×10^{-5} in human (Norden *et al.* 2001; Mori *et al.* 2017). We used an intermediate value of 0.1 mg l^{-1} (0.625 nM).

In the absence of mouse-specific data, the filtrate concentration of $\beta 2\text{m}$ was estimated as the product of its plasma concentration and sieving coefficient in human (Norden *et al.* 2001; Drueke & Massy, 2009), that is, $1.5 \text{ mg l}^{-1} \times 0.91 = 1.37 \text{ mg l}^{-1}$ (117.7 nM).

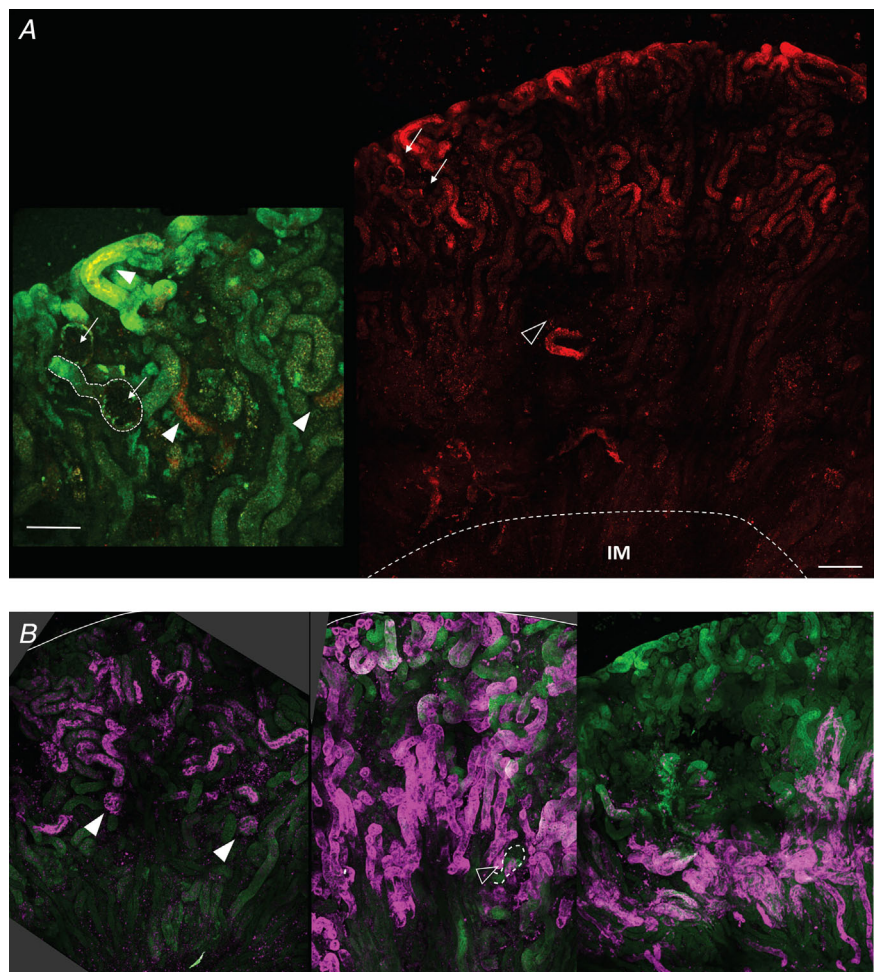
Results

Axial uptake of a fluid-phase marker

We observed that 10 kD Alexa Fluor-568 dextran acutely delivered into the circulation of mice by intracardiac injection was preferentially recovered distal to the S1 segment of the PT (Fig. 1). In isolated nephrons, we observed transitions in the level of dextran recovery along individual nephrons. While uptake varied considerably between nephrons consistent with previous

Figure 1. Fluorescence image of mouse kidney injected with dextran showing preferential uptake of dextran in proximal tubule S2 segments

A, maximum projection of large tilescan image showing distribution of injected Alexa Fluor 568 conjugated dextran (10 kDa). Arrows indicate 2 glomeruli with proximal tubule S1 segments revealing little to no uptake of dextran. Open arrowhead indicates location of arcuate artery. Dashed line indicates border between inner and outer medulla. Scale bar $250 \mu\text{m}$. Inset to left; $\times 2$ magnification of same region with 2 glomeruli similarly marked, and dashed outline of S1. Green autofluorescence is overlaid to confirm areas of greater dextran uptake (arrowheads). Scale bar $100 \mu\text{m}$. **B**, three panels from left to right showing distribution of S1 (SGLT2), S2 (OAT1) and S3 (AQP-4) segments in maximum projection large tilescan images. Filled arrowheads in left panel mark glomeruli and associated S1 segments positive for SGLT2. Open arrowhead in middle panel points to a glomerulus and associated S1 segment without OAT1 staining (outlined by the dashed line), consistent with its use as a marker of S2 segments. Right panel shows positive proximal tubule AQP4 staining primarily around the corticomedullary junction consistent with S3 distribution. Scale in **B** is equivalent to scale in right-side panel in **A**



reports (Schuh *et al.* 2018), the accumulation of dextran in deeper regions of the cortex near the medullary boundary (defined by the arcuate artery in Fig. 1A) suggests preferential retrieval within the S2 segment. Low magnification tilescan images of fixed kidney sections stained with markers for S1, S2 and S3 segments confirmed that dextran uptake most closely matched the S2 staining profile (Fig. 1B). Quantitative estimates of dextran intensity in this compartment relative to S1 segments (PT as it first emerges from Bowman's capsule judged by 3D projections) suggest a 7-fold enhancement of fluid-phase uptake. The increased uptake of dextran in S2 is consistent with recent studies suggesting that more distal regions of the PT harbour a reserve capacity that can be accessed when higher concentrations of ligand are filtered (Schuh *et al.* 2018; Christensen *et al.* 2021).

Competitive binding by filtered ligands at normal versus nephrotic concentrations

Under normal conditions, retrieval of albumin in the PT may be reduced due to competitive inhibition for uptake by lower molecular mass filtered proteins that enter the tubule lumen at relatively high concentration. Based on studies in Dent1 disease patients, $\beta 2m$ is predicted to be the most abundant tubular protein in the filtrate (Edwards *et al.* 2021), with an estimated concentration of 1.4 mg l^{-1} (121 nM). To evaluate whether $\beta 2m$ inhibits uptake of albumin, we tested the effect of increasing concentrations of fluorescently tagged purified $\beta 2m$ on the uptake of albumin by OK cells. As shown in Fig. 2A, even high concentrations of $\beta 2m$ (2 mg l^{-1} ; 172 nM) had no effect on the uptake of 25 mg l^{-1} (382 nM) albumin.

In addition to the recovery of normally filtered proteins, megalin and cubilin receptors also bind to proteins with

higher molecular mass than albumin that are normally efficiently excluded from the tubular filtrate. When the integrity of the glomerular barrier is compromised, increased levels of these proteins also gain access to the tubular filtrate, and may compete with albumin for uptake. Immunoglobulins are the most abundant plasma protein after albumin, with an estimated concentration in mouse plasma of 2500 mg l^{-1} (Klein-Schneegans *et al.* 1989; Honjo *et al.* 2012) (compared with $25000\text{--}30000 \text{ mg l}^{-1}$ for albumin) (Mori *et al.* 2017; Weyer *et al.* 2018). The normal tubular concentration of IgG was estimated to be 0.1 mg l^{-1} under normal conditions (see Methods), and 2 mg l^{-1} under nephrotic conditions. In a previous study, IgG was found to inhibit albumin uptake only at very high (supraphathologic) concentrations (200 mg l^{-1}) (Zhai *et al.* 2000). Consistent with this, we found no effect of increasing amounts of IgG (0, 20 or 200 mg l^{-1}) on the uptake of fluorescent albumin (Fig. 2B).

Baseline albumin excretion

All model parameter values were specified based on experimental data (Table 1), with the exception of V_{\max} values. To determine V_{\max}^{cub} and V_{\max}^{meg} , we fitted the model to the data of Weyer *et al.* (2011, 2018) as follows. Their results suggest that the fractional excretion of albumin (FE_{alb}) in WT mice is around 3%, assuming a glomerular filtration rate (GFR) of $280 \mu\text{l min}^{-1}$ and a creatinine excretion of 0.4 mg day^{-1} (Meneton *et al.* 2000; Dunn *et al.* 2004). Relative to WT mice, albumin excretion was 22-fold higher in megalin/cubilin KO mice (Weyer *et al.* 2018), 8.5-fold higher in cubilin KO mice and 15-fold higher in megalin KO mice (Weyer *et al.* 2011). Gene inactivation in KO mice was 85–92% efficient (Weyer *et al.* 2018).

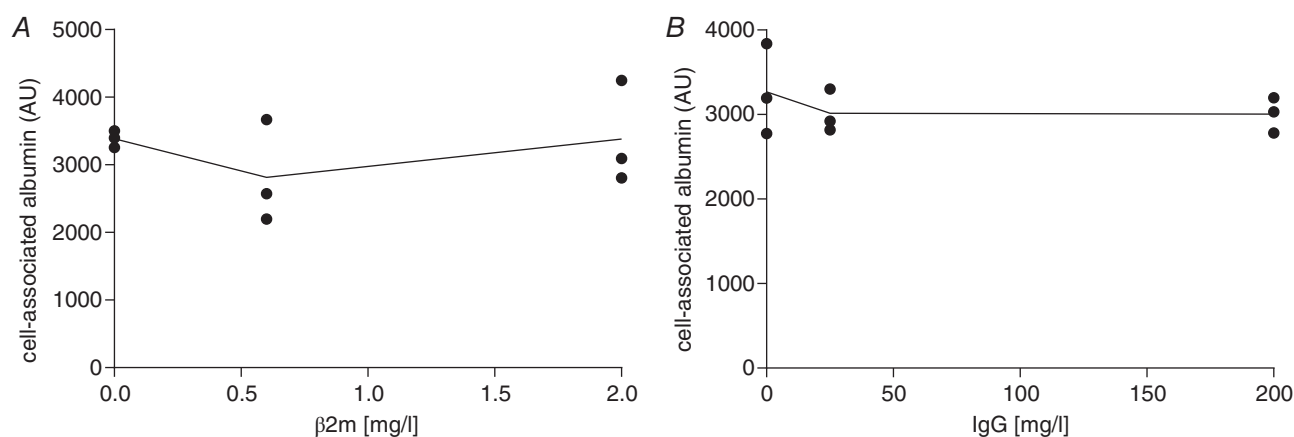


Figure 2. Competition for albumin uptake by $\beta 2$ -microglobulin ($\beta 2m$) and IgG

OK cells cultured on transwell supports under orbital shear stress were incubated with 25 mg l^{-1} Alexa Fluor-488 albumin and the indicated concentrations of $\beta 2m$ (A) or IgG (B) for 15 min at 37°C . Cells were solubilized and cell-associated fluorescence quantified by spectrofluorimetry. The points show albumin uptake (one filter per point) in three independent experiments and the line represents the mean of the data.

Table 2. Predicted albumin uptake under normal filtration conditions

	Fractional excretion	Total uptake (mg day ⁻¹)	% via cubilin	% via megalin	% via fluid phase
Base case	3.05%	0.823	74.9	25.0	0.12
Cubilin KO (90%)	25.3%	0.634	16.5	83.1	0.42
Cubilin + megalin KO (90%)	73.2%	0.227	61.5	36.6	1.9
No cubilin	30.6%	0.589	0	99.5	0.50
No megalin	9.9%	0.765	99.8	0	0.18
No cubilin + no megalin	99.4%	0.005	0	0	100

Albumin filtration equals $2 \text{ mg l}^{-1} \times 295 \mu\text{l min}^{-1} = 0.590 \mu\text{g min}^{-1}$, or $0.848 \text{ mg day}^{-1}$.

Since knocking out megalin impacts endocytic pathway integrity and prevents cubilin-mediated endocytosis, we did not simulate albumin handling in megalin KO mice. We sought to find values of $V_{\text{max}}^{\text{cub}}$ and $V_{\text{max}}^{\text{meg}}$ that yield $\text{FE}_{\text{alb}} \sim 3\%$ in WT mice, about 8.5 times higher ($\sim 25\%$) in cubilin KO mice, and about 22 times higher ($\sim 70\%$) in megalin/cubilin KO mice. In these KO simulations, the cubilin and megalin V_{max} were reduced by 90% to account for partial inactivation (Weyer *et al.* 2018). With $V_{\text{max}}^{\text{cub}} = 2.27$ and $V_{\text{max}}^{\text{meg}} = 6.38 \text{ fmol s}^{-1} \text{ mm}^{-2}$, the predicted FE_{alb} was 3.05%, 25.3% and 73.2%, respectively (Table 2).

Respective contributions of megalin versus cubilin under normal conditions

Predicted albumin mass flow and concentration profiles along short (SLN) and long (LLN) loop nephrons are shown in Fig. 3. The rate of albumin retrieval decreases along the PT and becomes almost negligible in S3: 79.3% of retrieved albumin is reabsorbed in S1, 20.3% in S2 and 0.4% in S3 (Table 3). Since water reabsorption is faster than albumin uptake in S3, C_{alb} is predicted to increase slightly along this sub-segment.

Shown in Fig. 4 are the fluxes of albumin across each pathway under normal conditions. The model predicts that overall, 74.9% of retrieved albumin is reabsorbed via cubilin, 25.0% via megalin and 0.12% via fluid-phase uptake (Table 3). In S1, 4 times more albumin is reabsorbed via cubilin than via megalin, but the relative contributions of cubilin and megalin become similar in S2 and S3. Since LLNs have a longer S1 relative to SLNs (Christensen *et al.* 2021), they reabsorb more albumin via cubilin along the PT (77.5% in LLNs vs. 73.4% in SLNs).

Albumin excretion in nephrotic mice

We then simulated the impact of nephrotic syndrome on the axial uptake of albumin, using parameters obtained from two nephrotic mouse models (Weyer *et al.* 2018; Butt *et al.* 2020). The concentration of albumin in the filtrate was computed as the product of plasma albumin (9.1 g l^{-1})

and the albumin sieving coefficient (0.08) in podocin KO mice (Weyer *et al.* 2018), that is, 728 mg l^{-1} , a 364-fold increase relative to its normal value (2 mg l^{-1}). We also assumed a 35% decrease in GFR (Butt *et al.* 2020).

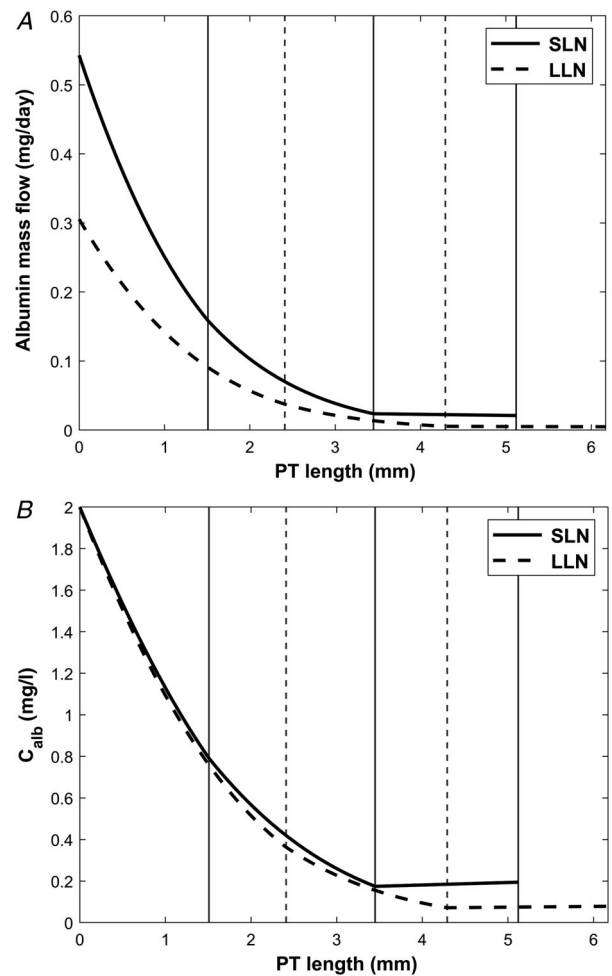


Figure 3. Predicted albumin profiles under normal conditions: albumin mass flow (A) and albumin concentration (C_{alb}) (B) in the PT lumen of short (SLN) and long (LLN) loop nephrons
The vertical lines denote the boundaries between S1–S2 and S2–S3 for SLN (continuous lines) and LLN (dashed lines).

As described in Methods, our model accounts for the effects of abundant plasma proteins that may affect albumin endocytosis, namely IgG and β 2m. We assumed that the plasma concentration of IgG decreases 10-fold in nephrotic mice (Weyer *et al.* 2018), and that the sieving coefficient of IgG increases by a factor of 213, that is 5-fold less than that of albumin based on clearance data in nephrotic humans (Guasch *et al.* 1993; Blouch *et al.* 1997). With these hypotheses, the filtrate concentration of IgG was estimated as 2.1 mg l^{-1} . Since β 2m is almost freely filtered under normal conditions, its concentration in the filtrate does not increase much in nephrotic mice;

Table 3. Predicted contributions of three pathways to albumin uptake under normal conditions

	Delivery	Uptake	Uptake via cubilin	Uptake via megalin	Uptake via fluid phase
S1	0.848	0.653	0.520	0.132	0.0006
S2	0.195	0.167	0.095	0.072	0.0004
S3	0.028	0.003	0.001	0.002	0.0000
Total	0.025	0.823	0.616	0.206	0.0010

(end of PT)

All values are in mg day^{-1} . Values correspond to mean of SLNs and LLNs assuming a 64:36 ratio.

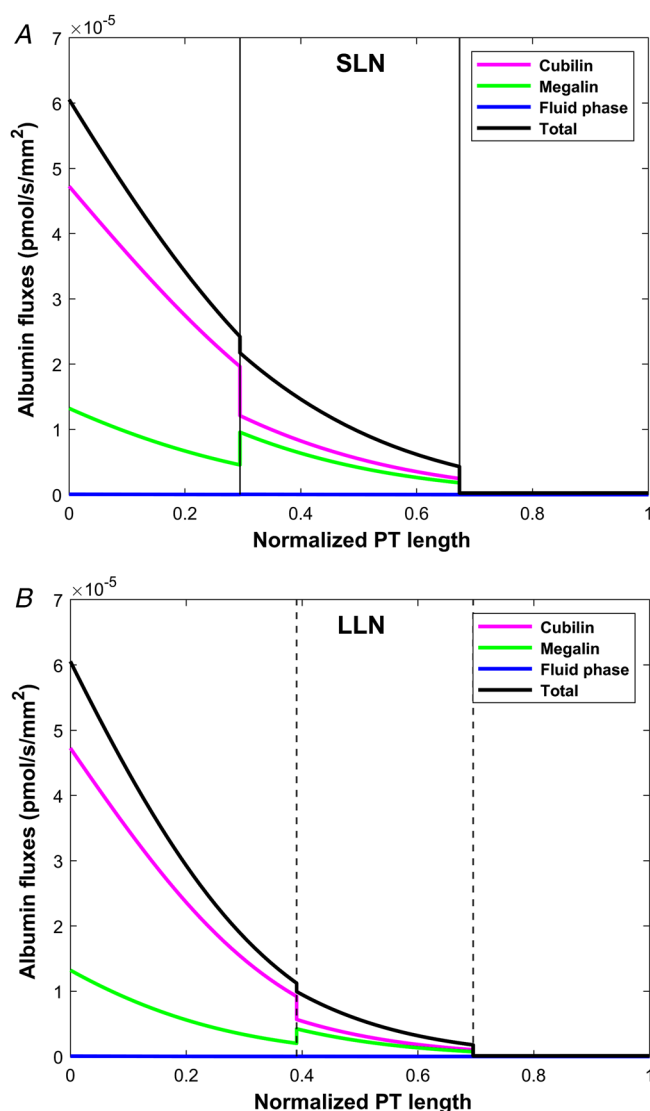


Figure 4. Predicted albumin fluxes per nephron along SLN (A) and LLN (B) under normal conditions

The x-axis represents the axial coordinate divided by total PT length, and the vertical lines denote the boundaries between S1–S2 and S2–S3. The bulk of normally filtered albumin is retrieved in S1, via cubilin. [Colour figure can be viewed at wileyonlinelibrary.com]

we set it equal to its plasma concentration, 1.5 mg l^{-1} . Decreases in GFR have been associated with increases in fractional water reabsorption (Landwehr *et al.* 1968). However, varying f_w in our model has a small impact on model predictions (results not shown) so we maintained it constant.

Assuming no loss of nephrons, the single nephron GFR (SNGFR) was set equal to 65% of its basal value. Absent changes in V_{max} , the predicted excretion of albumin in nephrotic mice was 110 mg day^{-1} , a 4200-fold increase relative normal conditions, which is higher than the 3000-fold increase in podocin KO mice reported by Weyer *et al.* (2018). This discrepancy may be due in part to effects of glomerular dysfunction and heavy proteinuria on the expression or distribution of megalin/cubilin, as well as to challenges in reliably quantifying urinary albumin values (Weisz & Baty, 2018). Additionally, the extent to which GFR and SNGFR were impacted in podocin KO mice was not reported or is not known (see below).

Figure 5 depicts the predicted variations in albumin mass flow and concentration along SLN and LLN, and Fig. 6 shows the corresponding fluxes of albumin across each pathway. Under nephrotic conditions, the concentration of albumin is >10-fold higher than its affinity to cubilin, and megalin-mediated endocytosis constitutes the predominant albumin uptake mechanism: 31.1% of retrieved albumin is reabsorbed via cubilin, 67.4% via megalin and 1.5% via fluid-phase uptake. Since megalin expression is highest in S2, albumin uptake is highest in that segment as well: 41.4% of retrieved albumin is reabsorbed in S1, versus 55.5% in S2 and 3.1% in S3 (Table 4).

Determinants of uptake capacity

A key determinant of uptake capacity is the maximum reabsorption rate via cubilin and megalin, the only fitted parameter in this model. To examine the sensitivity of our predictions to this parameter, we assessed the impact

Table 4. Predicted contributions of three pathways to albumin uptake under nephrotic conditions

	Delivery	Uptake	Uptake via cubilin	Uptake via megalin	Uptake via fluid phase
S1	200.7	37.6	17.6	19.6	0.39
S2	75.7	50.3	10.2	39.2	0.91
S3	42.8	2.9	0.4	2.4	0.06
Total	110.0 (end of PT)	90.7	28.2	61.2	1.36

All values are in mg day^{-1} and based on a 35% decrease in GFR. Values correspond to mean of SLNs and LLNs assuming a 64:36 ratio.

of varying V_{\max} on model results. Because megalin and cubilin are believed to traffic co-ordinately, in this analysis we adjusted V_{\max} to the same extent for both receptors. Our results indicate that V_{\max} would have to be at least 8 times lower than our baseline value for the majority of

albumin to be retrieved in S2 (as opposed to S1) under normal conditions. Conversely, V_{\max} would have to be at least 2.6 times higher than our baseline value for the majority of albumin to be retrieved in S1 (as opposed to S2) under nephrotic conditions.

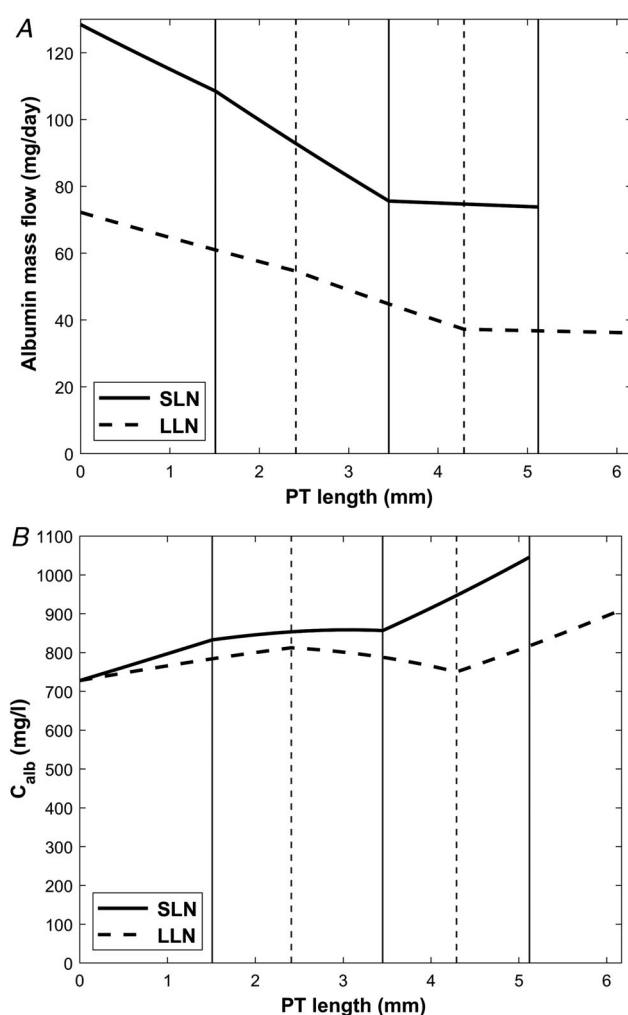


Figure 5. Predicted albumin profiles under nephrotic conditions: albumin mass flow (A) and albumin concentration (B) in the PT lumen

The vertical lines denote the boundaries between S1–S2 and S2–S3 for SLN (continuous lines) and LLN (dashed lines).

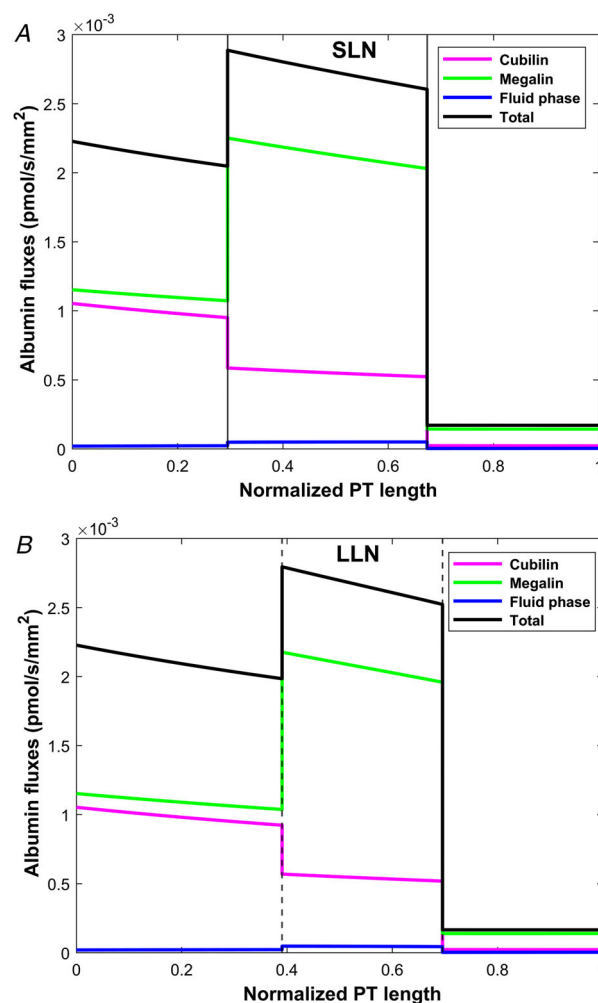


Figure 6. Predicted albumin fluxes per nephron along SLN (A) and LLN (B) under nephrotic conditions

The x-axis represents the axial coordinate divided by total PT length, and the vertical lines denote the boundaries between S1–S2 and S2–S3. In the nephrotic state, the bulk of filtered albumin is retrieved in S2, via megalin. [Colour figure can be viewed at wileyonlinelibrary.com]

Table 5. Sensitivity of predicted albumin uptake under nephrotic conditions to model parameters

	Filtration (mg day ⁻¹)	Fractional excretion	Total uptake (mg day ⁻¹)	% via S1	% via S2	% via S3
Impact of GFR						
No decrease in GFR	308.8	65.2%	107.3 31.0% via cubilin, 67.6% via megalin, 1.4% via fluid-phase	41.8	55.1	3.1
35% decrease in GFR	200.7	54.8%	90.7 31.1% via cubilin, 67.4% via megalin, 1.5% via fluid-phase	41.4	55.5	3.1
50% decrease in GFR	154.4	46.2%	83.0 31.3% via cubilin, 67.2% via megalin, 1.5% via fluid-phase	41.4	55.4	3.2
Impact of filtrate concentration						
10-fold increase in filtrate concentration*	2007	93.5%	129.5 23.3% via cubilin, 62.6% via megalin, 14.1% via fluid-phase	38.0	58.4	3.6
Direct contribution of receptors						
No cubilin*	200.7	67.8%	64.6 97.6% via megalin, 2.4% via fluid-phase	31.3	64.6	4.0
No megalin*	200.7	85.0%	30.1 94.4% via cubilin, 5.6% via fluid-phase	60.0	38.3	1.7
No cubilin, no megalin*	200.7	99.1%	1.9 100% via fluid-phase	23.0	70.9	6.1

* Assuming a 35% decrease in GFR.

In addition to receptor membrane abundance, uptake capacity is also a function of filtrate concentration and fluid flow. To further assess the robustness of our qualitative predictions, we examined the impact of filtrate concentration and GFR on albumin uptake under nephrotic conditions. Whereas fluid-phase uptake increases in direct proportion to filtrate concentration, receptor-mediated endocytosis eventually becomes concentration-independent and reaches a plateau. In our model, receptor-mediated endocytosis becomes saturated when the filtrate concentration of albumin is increased 10 times above its baseline value of 728 mg l⁻¹ (nephrotic conditions). Under these supra-pathologic conditions, more albumin is retrieved in S2 via the fluid phase (12.8 mg day⁻¹) than via cubilin (10.9 mg day⁻¹), and fluid phase accounts for 14% of total uptake (Table 5).

The extent to which the GFR decreases in nephrotic mice will vary with disease model and the progression of kidney injury. In the simulations above, we assumed a 35% decrease. Here, we considered two other scenarios: no change or a 50% decrease in GFR. Corresponding results, shown in Table 5, indicate that the fractional uptake of albumin via cubilin and megalin does not vary by more than 0.5% in these other cases. In other words, our prediction that the bulk of albumin uptake shifts towards S2 and megalin under nephrotic conditions is not sensitive to assumed GFR values.

Direct contributions of cubilin and megalin

In the following simulations, we abolished the direct effect of binding to cubilin, megalin or both on albumin uptake. Since the absence of megalin alters the integrity of the other uptake pathways, the megalin-mediated uptake component is impossible to determine experimentally.

As shown in Fig. 7, without cubilin-mediated uptake, albumin retrieval is predicted to decrease by ~30%, as megalin-mediated uptake increases by ~0.4 (normal) and 2.0 (nephrotic) mg day⁻¹ in compensation (Tables 2 and 5). Accordingly, the model predicts a large shift in albumin uptake from S1 towards mostly S2 (where megalin is more prominently expressed) under normal filtration conditions (Fig. 7A). This shift is less pronounced under nephrotic conditions (Fig. 7B), since S2 is already the sub-segment with the highest contribution when all three pathways are active.

Conversely, without megalin-mediated uptake, albumin uptake via cubilin increases only by ~0.2 mg day⁻¹ under both conditions (Tables 2 and 5). In other words, the ability of cubilin to counterbalance the absence of megalin is negligible under nephrotic conditions.

When direct cubilin- and megalin-mediated endocytosis are both disabled, fluid-phase uptake increases 5-fold under normal conditions, and by ~40% under nephrotic conditions. The increase occurs mostly in S2,

because of rising concentrations along the tubule. Under normal conditions, albumin uptake via fluid phase is predicted to be 3.5 times greater in S2 than in S1.

Axial uptake profile of other filtered proteins

We measured the concentration-dependent uptake of IgG and β 2m to estimate their uptake affinities in order to predict the axial uptake profile of these two proteins under normal *versus* nephrotic conditions. The profiles we obtained for the concentration-dependent uptake of β 2m and IgG by OK cells is consistent in both cases with the presence of a single low-affinity, high-capacity site for uptake of these ligands (Fig. 8A and B). Although β 2m

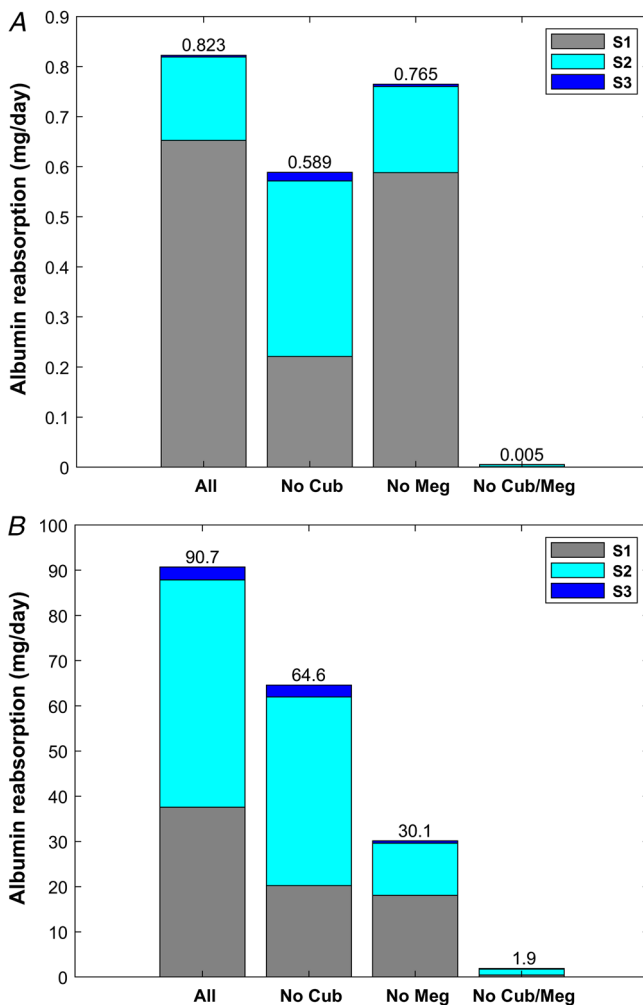


Figure 7. Predicted role of individual receptor components in albumin recovery, under normal (A) and nephrotic conditions (B): with all three pathways (All), without cubilin-mediated uptake (No Cub), without megalin-mediated uptake (No Meg), and without cubilin- and megalin-mediated uptake (No Cub/Meg)

[Colour figure can be viewed at wileyonlinelibrary.com]

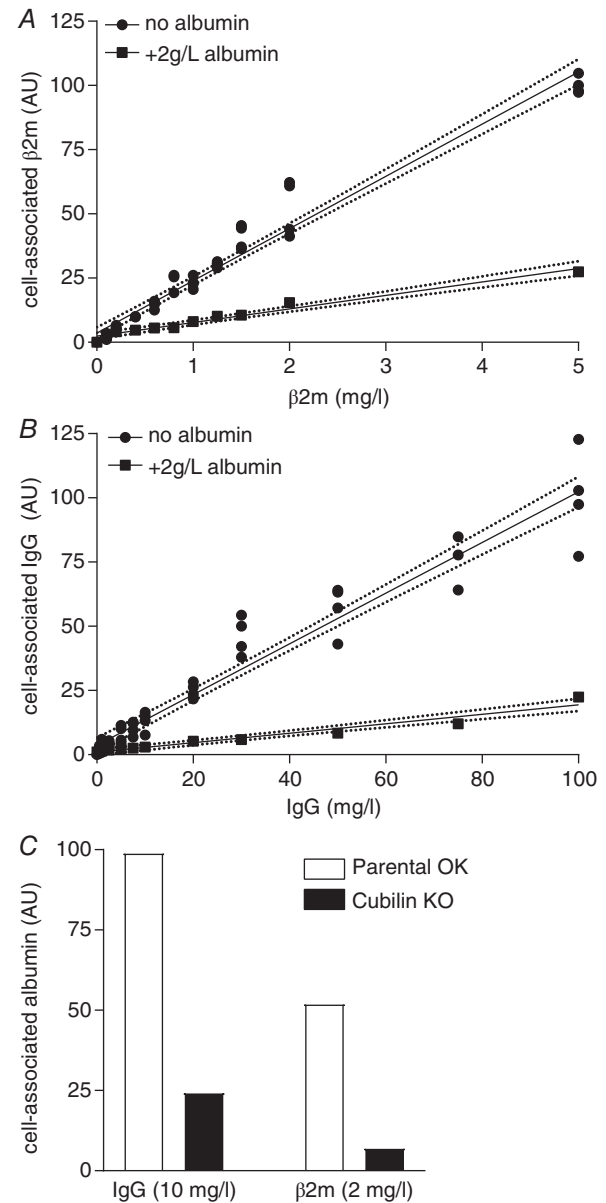


Figure 8. Dose-dependent uptake of β 2m and IgG in PT cells. A and B, OK cells cultured on transwell supports under orbital shear stress were incubated with the indicated concentrations of Alexa Fluor-647 conjugated β 2m (A) or IgG (B) for 15 min at 37°C. Cells were solubilized and cell-associated fluorescence quantified (circles). Individual data from four samples in two independent experiments are plotted. The fluid phase uptake component was estimated by inclusion of 2 g l⁻¹ albumin in one filter at each ligand concentration (squares). Linear regression (continuous line) with 95% confidence interval (dotted lines) is consistent with linear uptake across the concentration range tested ($R^2 = 0.963$ and 0.941 for β 2m and IgG, respectively). C, control (white bars) or CRISPR/Cas9 Cubin KO OK cells (black bars) were incubated as above with 2 mg l⁻¹ β 2m or 10 mg l⁻¹ IgG and cell-associated fluorescence was quantified. Data from an individual point for each condition normalized to the IgG control are plotted for simplicity; however, comparable results were obtained using several other conditions for each ligand.

and IgG have been reported to bind weakly to megalin (Leheste *et al.* 1999; Bryniarski *et al.* 2021), we found that in both cases, ligand uptake was dramatically blunted in CRISPR/Cas9 *Cubn* knockout OK cells (Fig. 8C). The contribution of fluid phase uptake was estimated by inclusion of 2 g l⁻¹ albumin as a competitive inhibitor. For β 2m, no saturation was observed at up to 5 mg l⁻¹ (>3-fold the estimated serum concentration) (Fig. 8A), which is consistent with the K_m value of 4.6 mg l⁻¹ reported by Leheste *et al.* (1999). For IgG, uptake was linear at concentrations up to 100 mg l⁻¹, well above the estimated nephrotic tubular concentration of 2 mg l⁻¹ (Fig. 8B). To quantify inhibition by albumin, we used concentrations of albumin consistent with normally filtered levels (25 mg l⁻¹) and proteinuric conditions (375 and 750 mg l⁻¹), and measured the effect on uptake of β 2m (0.6, 2 and 5 mg l⁻¹) or IgG (0.5, 10 and 100 mg l⁻¹). Whereas even low concentrations of albumin (25 mg l⁻¹) significantly inhibited IgG uptake, β 2m was competed with only by nephrotic concentrations of albumin (Fig. 9). These data are consistent with a previous study where albumin was demonstrated to inhibit the uptake of IgG by OK cells (Nagai *et al.* 2011).

Based on the results of Fig. 8 and previous findings (Leheste *et al.* 1999), the affinity of cubilin to β 2m was set to 4.6 mg l⁻¹ (420 nM) and that to IgG was set to 100 mg l⁻¹ (625 nM) in the computational model. To verify that these assumptions are consistent with the remainder of our data, we ran simulations to mimic the competition experiments (Figs 2 and 9). Model predictions reproduced the experimental data very well (results not shown).

We then used the model to examine the spatial distribution of β 2m and IgG uptake along the PT. Predicted β 2m and IgG concentration profiles in normal and nephrotic conditions are shown in Fig. 10. Note

that the amount of filtered β 2m decreases under the nephrotic conditions we examined, because the filtrate concentration increase (10%) is smaller than the GFR decrease (35%). The predicted fractional excretions of β 2m and IgG are, respectively, 2.5% and 8.2% in normal conditions, and 74.8% and 82.0% in nephrotic conditions (Table 6). The contribution of fluid-phase uptake is <0.5% in normal conditions and increases to 3–5% under nephrotic conditions. In the latter case, uptake via cubilin is predicted to be slower than water reabsorption, hence the increase in ligand concentration along the PT (Fig. 10B). As shown in Fig. 11, 80–85% of β 2m and IgG are reabsorbed in S1 in normal conditions, *versus* 15–20% in S2 and <1% in S3 (Table 6). The contribution of S2 becomes larger (~40%) in nephrotic conditions (Fig. 11).

We also examined the effects of abolishing cubilin-mediated uptake. In the absence of cubilin, the urinary excretion of IgG and β 2m is predicted to increase by a factor of 12 and 39, respectively, under normal conditions (*vs.* 10-fold for albumin). Under nephrotic conditions, abolishing cubilin-mediated uptake is predicted to raise the urinary excretion of IgG and β 2m by 20–30% (*vs.* 24% for albumin). Without cubilin-mediated uptake, fluid-phase endocytosis of IgG and β 2m is predicted to increase 4- to 7-fold (0.06 to 0.26 μ g day⁻¹ for IgG, 0.5 to 3.5 μ g day⁻¹ for β 2m) under normal conditions, and by 0.6–0.7 μ g day⁻¹ (4.9 to 5.5 μ g day⁻¹ for IgG, 3.2 to 3.9 μ g day⁻¹ for β 2m) under nephrotic conditions. Thus, the capacity of fluid-phase endocytosis is also limited for IgG and β 2m.

Discussion

The model described herein predicts the rates of albumin uptake across three distinct pathways in the mouse PT,

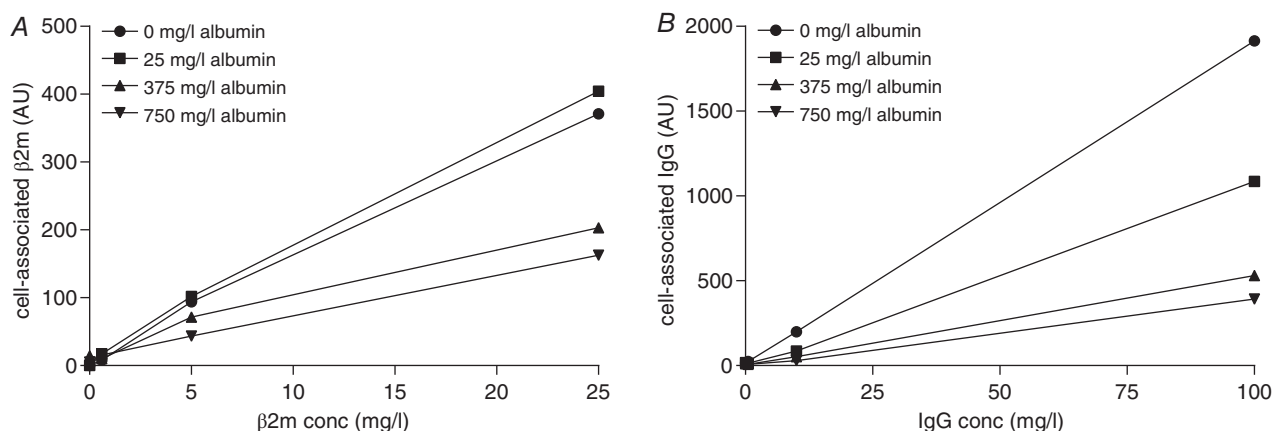


Figure 9. Albumin inhibition profile of β 2m and IgG in PT cells

OK cells cultured on transwell supports under orbital shear stress were incubated with the indicated concentrations of Alexa Fluor-647 conjugated β 2m (A) or IgG (B) and 0, 25, 375 or 750 mg l⁻¹ albumin for 15 min at 37°C. Cells were solubilized and cell-associated fluorescence quantified.

Table 6. Predicted uptake of IgG and β 2m in the proximal tubule

	Filtration (mg day ⁻¹)	FE (%)	Uptake (mg day ⁻¹) (%) via cubilin	% via S1	% via S2	% via S3
IgG						
Normal	0.042	8.2%	0.039(99.8%)	78.4	21.1	0.5
Nephrotic	0.588	82.0%	0.106(95.4%)	56.3	41.7	2.0
β 2m						
Normal	0.579	2.5%	0.565(99.9%)	86.5	13.3	0.2
Nephrotic	0.414	74.8%	0.104(96.9%)	57.9	40.2	1.8

in normal and nephrotic states. It includes quantitative proteomic data (Limbutara *et al.* 2020) to estimate receptor abundance, data from OK cells to estimate receptor-specific affinity values (Ren *et al.* 2020), as well

as data from KO models to distinguish between the contributions of megalin *versus* cubilin *in vivo* (Weyer *et al.* 2011; Weyer *et al.* 2018). It includes moreover new estimates of binding affinity and measurements of competitive inhibition for abundant serum/filtrate

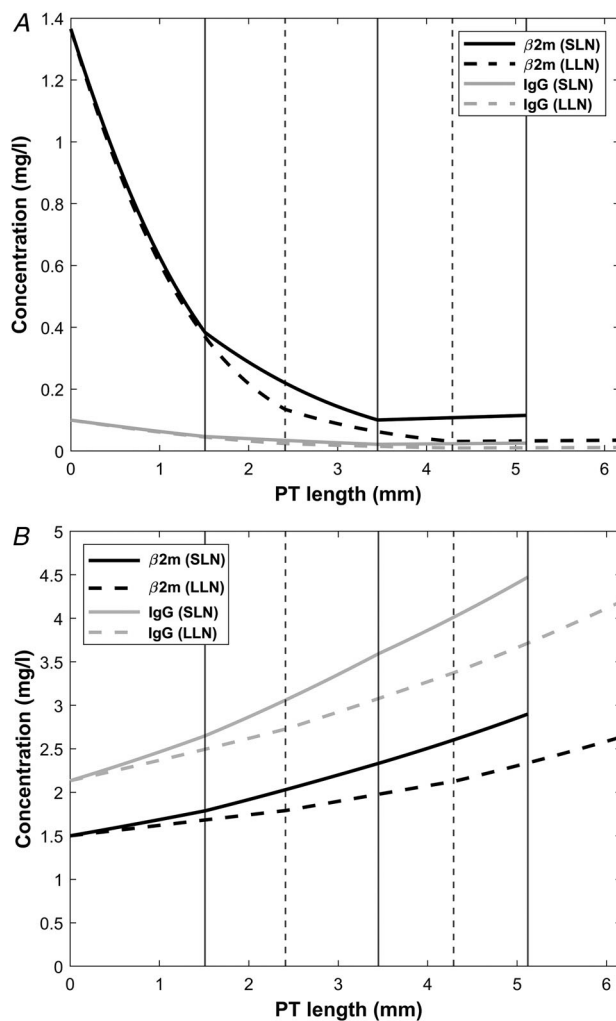


Figure 10. Predicted IgG and β 2m concentrations along the PT lumen under normal (A) and nephrotic (B) conditions
The vertical lines denote the boundaries between S1–S2 and S2–S3 for SLN (continuous lines) and LLN (dashed lines).

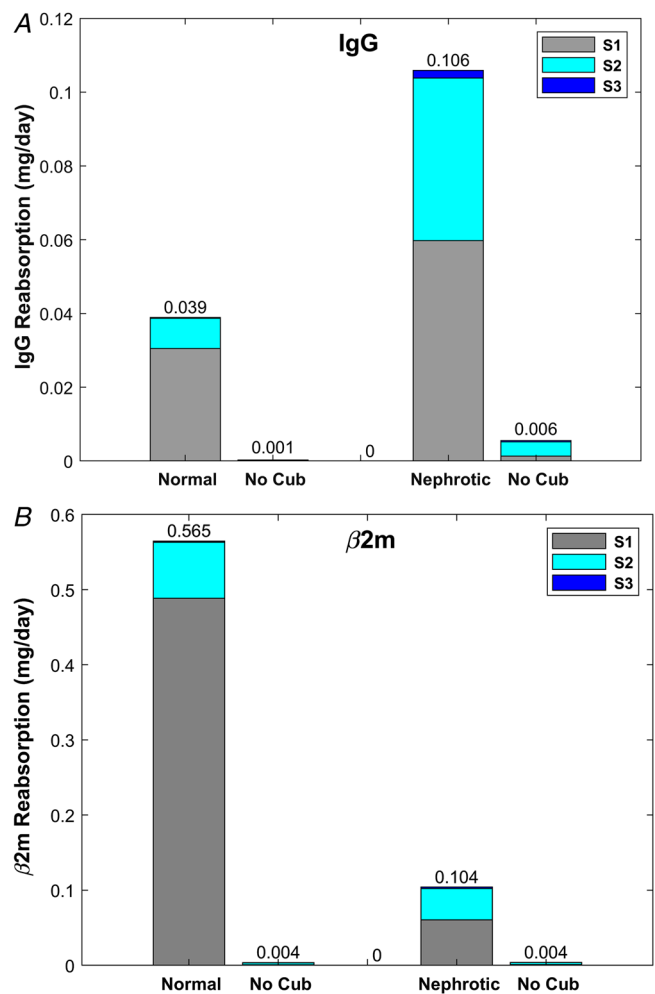


Figure 11. Predicted uptake of IgG (A) and β 2m (B) under normal and nephrotic conditions, with and without cubilin-mediated uptake
[Colour figure can be viewed at wileyonlinelibrary.com]

proteins. We have also compared the normal and nephrotic axial uptake profile of albumin with that of other proteins with distinct sieving coefficients and binding affinities for cubilin. To our knowledge, this is the first mathematical model to reveal sub-segment-specific contributions to albumin uptake along the PT.

Our model reveals several striking differences in the recovery of albumin between normal and nephrotic conditions. Under normal conditions, the majority of albumin is recovered in the S1 segment, consistent with the rapid uptake in the early PT predicted in previous models of albumin recovery in human and mouse kidney (Lazzara & Deen, 2007; Gliozzi *et al.* 2020; Edwards *et al.* 2021). By contrast, under nephrotic conditions, albumin is recovered primarily in the S2 segment. This shift in axial recovery reflects both the high concentration of ligand that enters this segment and the relative abundance of megalin, which mediates low-affinity, high-capacity uptake of albumin. Thus, while 74.9% of normally filtered albumin is reabsorbed via cubilin, megalin-mediated recovery accounts for 67.4% of recovery under the nephrotic conditions we modelled. This observation is consistent with previous experimental data in nephrotic mice that demonstrate a preferential requirement for megalin *versus* cubilin expression in the uptake of albumin (Ren *et al.* 2020). Additionally, the data are generally consistent with the description of a 'reserve' recovery pathway for filtered retinol binding protein 4 and $\beta 2m$ in nephrotic mouse kidneys (Christensen *et al.* 2021). Finally, the dearth of uptake in S3 segments that we modelled is consistent with the paucity of endocytic compartments described in ultrastructural studies of this segment (Christensen *et al.* 2012b; Christensen *et al.* 2021). Rigorously controlled imaging studies to quantify the axial distribution of internalized albumin and other filtered ligands in PT sub-segments under nephrotic compared with normal conditions are needed to verify our predictions.

This model provides a kinetic rationale for why proteinuria stemming from a tubular defect (such as in Dent disease, Lowe syndrome, or cubilin KO) can occur when normally filtered levels of albumin are inefficiently recovered even though there is a large excess in potential PT uptake capacity. Uptake capacity depends on amount of ligand, binding kinetics and receptor abundance. At low albumin concentrations, uptake is rate-limited by the rate at which ligands bind to their receptors (specifically, by the concentration-to-affinity ratio). At high (nephrotic) albumin concentrations, binding sites approach saturation and uptake becomes rate-limited by receptor abundance. This explains why uptake can increase >25-fold under nephrotic conditions: as albumin concentration increases, binding kinetics cease to be rate-limiting; eventually, the availability of binding sites becomes the determining factor.

In proteinuria stemming from a glomerular defect, our model suggests that drugs that lower GFR, such as calcineurin inhibitors, may reduce the absolute urinary excretion of albumin to a greater extent than the reduction in GFR, all else remaining constant. As shown in Table 5, a 35% decrease in GFR in nephrotic mice is predicted to reduce albumin excretion from 202 to 110 mg day⁻¹, a 45% decrease. This dis-coordinated effect occurs because reducing the (single nephron) GFR increases solute residence time in the tubule and enhances uptake, and it may contribute to the efficacy of such drugs.

Our simulations also enabled us to estimate the contribution of fluid-phase uptake to the recovery of albumin and other filtered ligands. While PT cells do not have a dedicated endocytic pathway for fluid-phase uptake, a significant volume of fluid is expected to accompany the robust membrane internalization observed in rat PT (Birn *et al.* 1993) and which was estimated in OK cells to represent 0.6% of the cell volume per minute (Gekle *et al.* 1995). Fluid-phase uptake was suggested to represent a major pathway for retrieval of high concentrations of albumin in microdissected rabbit nephrons (Park & Maack, 1984). Moreover, quantification of dextran internalized by PT cells after injection in mice revealed an ~7-fold increase in the relative uptake of this fluid-phase marker in S2 segments of the PT compared with S1 (Fig. 1), suggesting the possibility of robust concentration-dependent salvage of albumin via this pathway. While these observations led us to suggest the possibility that recovery of concentrated albumin in the fluid-phase might contribute significantly to albumin retrieval in nephrotic conditions (Weisz, 2021), our model here shows that receptor-mediated rather than fluid-phase uptake accounts for the vast majority of ligand recovery. Only 0.12% of normally filtered albumin was taken up in the fluid phase, and this increased to 1.5% under nephrotic conditions. In terms of total mass, the fluid-phase component of albumin uptake under the nephrotic conditions we modelled (1.36 mg day⁻¹) is slightly higher than *total* albumin uptake under normal conditions (0.82 mg day⁻¹). Whether the dramatic increase in the retrieval of dextran we observed in S2 compared with S1 segments reflects a more robust endocytic pathway due to higher megalin expression and/or a dramatic increase in concentration remains to be determined.

While the direct contribution of megalin receptors to albumin retrieval is impossible to determine experimentally, we were able to evaluate the relative contributions of cubilin *versus* megalin receptors on axial uptake of albumin using our model. Strikingly, knockout of cubilin is predicted to shift the bulk of albumin uptake from S1 to S2 (Fig. 7), a prediction that may be testable by quantitative imaging studies in mouse

models. In addition, the direct effects of megalin on normal albumin endocytosis are predicted to be relatively small, in contrast with the very substantial impact of knocking-down megalin (Weyer *et al.* 2011).

Our model distinguishes between SLNs and LLNs by considering their differences in length. As such, it predicts only small variations in their handling of albumin, such as higher concentrations at the exit in SLNs *versus* LLNs (Figs 3 and 5). Recent topographical studies of mouse kidney nephrons revealed three general arrangements of PTs differing in their positioning, length and tortuosity (Blanc *et al.* 2021). Further studies that enable discrimination and quantification of nephron sub-segments within each group may provide additional variables that can be included in later expansions of this model.

Importantly, our studies also highlight the differences in axial uptake patterns of different ligands. Concentration-dependent studies of IgG and β 2m endocytosis in OK cells were consistent with a single binding site for ligand uptake under physiological and pathophysiological conditions. Notably, uptake of both ligands was reduced drastically in *Cubn* KO cells, suggesting that their internalization is mediated primarily by CUBAM receptors. Moreover, uptake of β 2m and IgG was significantly inhibited by physiologically relevant concentrations of albumin, while neither ligand significantly impaired the uptake of albumin. Because of the heavy reliance on cubilin for uptake, predicted β 2m and IgG axial recovery profiles qualitatively resemble that of albumin under normal conditions. However, while the contribution of S2 to ligand retrieval is more significant under nephrotic conditions, it is not dominant for IgG and β 2m (as it is for albumin), since cubilin is more heavily expressed in S1. As a consequence, the concentration of both ligands is predicted to steadily increase along the PT axis under nephrotic conditions (Fig. 10). Though technically challenging, this could potentially be tested experimentally by micropuncture. Despite the increase in ligand concentration, the contribution of fluid-phase uptake to overall recovery remains small (<5% of total; Table 6).

We should note that our mouse model predicts that the fractional excretions of β 2m and albumin are comparable (2.5% *vs.* 3.0%). In contrast, data from *Dent1* patients suggest that the fractional excretion of β 2m may be 50 times lower than that of albumin (Edwards *et al.* 2021). This discrepancy could mean that our model assumes incorrect β 2m affinity values and/or does not account for all existing β 2m uptake pathways. Additional experimental data in a variety of mouse and cell models may help resolve these questions.

As with any model of kidney function, ours is limited by the challenges in obtaining quantitative data from human and animal studies. While many of the parameters for

our model were obtained from measurements in mice, in some cases only data from rats or humans were available. To assign expression values for megalin, cubilin and Dab2 to PT sub-segments, we utilized quantitative proteomic data from microdissected rat nephrons (Limbutara *et al.* 2020) rather than RNASeq data from microdissected mouse tubules (Chen *et al.* 2021). However, comparison of the transcriptomic profiles between the two species (Lee *et al.* 2015; Chen *et al.* 2021) suggests that megalin mRNA levels in mouse S2 segments are comparable to those of S1 in mouse PT, whereas they are higher in S2 *versus* S1 in the rat. Owing to the paucity of available data in mice, our model also assumes that SLNs and LLNs vary only in terms of their length. The heterogeneity in orientation and tortuosity of individual nephrons observed in recent studies using cleared and microdissected tissues suggests additional variations between uptake profiles in SLNs *versus* LLNs that we cannot yet account for (Woodhall *et al.* 1978; Schuh *et al.* 2018; Blanc *et al.* 2021). This may include variations in fluid reabsorption that could have significant effects on ligand uptake in our model.

In addition to variations in tubular water transport, intravital studies reveal considerable nephron-to-nephron variability in filtration rate (Peti-Peterdi *et al.* 2015). Furthermore, there is significant variability in the severity of disease within and between mouse models of nephrosis that prevents definitive assignment of SNGFR among other variables. This variability may be due in part to the influence of protein casts and fibrosis on hydrodynamics, as well as to signalling and inflammatory responses as kidney disease progresses. Our model also does not account for possible changes in axial endocytic capacity as disease progresses. Megalin, cubilin and Dab2 expression have been shown to vary temporally or spatially during disease progression, and differential effects on transcription of these proteins or changes in other components that drive ligand uptake could impact our model (Liu *et al.* 2015; Christensen *et al.* 2021). Such changes may contribute to the uptake of β 2m observed in the S3 segments of cystinotic mice and in podocin KO mice (Gaide Chevronnay *et al.* 2014; Christensen *et al.* 2021).

Our model represents a useful starting point to explain the remarkable ability of the PT to accommodate wide variations in filtered protein load. Some predictions of our model as noted above can be experimentally tested to confirm our assumptions. Additionally, the increasing availability of data from human patients and proteinuric disease animal models (Ma *et al.* 2016; Bedin *et al.* 2020), as well as advancements in quantitative approaches to measure uptake of filtered proteins *in vivo* (Martins *et al.* 2021) can be used to further refine our model of albumin uptake and expand it to include a broader spectrum of ligands.

References

- Bedin M, Boyer O, Servais A, Li Y, Villoing-Gaude L, Tete MJ, Cambier A, Hogan J, Baudouin V, Krid S, Bensman A, Lammens F, Louillet F, Ranchin B, Vigneau C, Bouteau I, Isnard-Bagnis C, Mache CJ, Schafer T, Pape L, Godel M, Huber TB, Benz M, Klaus G, Hansen M, Latta K, Gribouval O, Moriniere V, Tournant C, Grohmann M, Kuhn E, Wagner T, Bole-Feysot C, Jabot-Hanin F, Nitschke P, Ahluwalia TS, Kottgen A, Andersen CBF, Bergmann C, Antignac C & Simons M (2020). Human C-terminal CUBN variants associate with chronic proteinuria and normal renal function. *J Clin Invest* **130**, 335–344.
- Birn H, Christensen EI & Nielsen S (1993). Kinetics of endocytosis in renal proximal tubule studied with ruthenium red as membrane marker. *Am J Physiol* **264**, F239–F250.
- Blanc T, Goudin N, Zaidan M, Traore MG, Bienaime F, Turinsky L, Garbay S, Nguyen C, Burtin M, Friedlander G, Terzi F & Pontoglio M (2021). Three-dimensional architecture of nephrons in the normal and cystic kidney. *Kidney Int* **99**, 632–645.
- Blouch K, Deen WM, Fauvel JP, Bialek J, Derby G & Myers BD (1997). Molecular configuration and glomerular size selectivity in healthy and nephrotic humans. *Am J Physiol* **273**, F430–F437.
- Bryniarski MA, Zhao B, Chaves LD, Mikkelsen JH, Yee BM, Yacoub R, Shen S, Madsen M & Morris ME (2021). Immunoglobulin G is a novel substrate for the endocytic protein megalin. *AAPS J* **23**, 40.
- Butt L, Unnerso-Jess D, Hohne M, Edwards A, Binz-Lotter J, Reilly D, Hahnfeldt R, Ziegler V, Fremter K, Rinschen MM, Helmstadter M, Ebert LK, Castrop H, Hackl MJ, Walz G, Brinkkoetter PT, Liebau MC, Tory K, Hoyer PF, Beck BB, Brismar H, Blom H, Schermer B & Benzing T (2020). A molecular mechanism explaining albuminuria in kidney disease. *Nat Metab* **2**, 461–474.
- Chen L, Chou CL & Knepper MA (2021). A comprehensive map of mRNAs and their isoforms across all 14 renal tubule segments of mouse. *J Am Soc Nephrol* **32**, 897–912.
- Christensen EI, Birn H, Storm T, Weyer K & Nielsen R (2012a). Endocytic receptors in the renal proximal tubule. *Physiology* **27**, 223–236. <https://doi.org/10.1152/physiol.00022.2012>
- Christensen EI, Kristoffersen IB, Grann B, Thomsen JS, Andreasen A & Nielsen R (2021). A well-developed endolysosomal system reflects protein reabsorption in segment 1 and 2 of rat proximal tubules. *Kidney Int* **99**, 841–853.
- Christensen EI, Wagner CA & Kaissling B (2012b). Uriniferous tubule: structural and functional organization. *Compr Physiol* **2**, 805–861.
- Clark JZ, Chen L, Chou C-L, Jung HJ, Lee JW & Knepper MA (2019). Representation and relative abundance of cell-type selective markers in whole-kidney RNA-Seq data. *Kidney Int* **95**, 787–796.
- Dachy A, Paquot F, Debray G, Bovy C, Christensen EI, Collard L & Jouret F (2015). In-depth phenotyping of a Donnai-Barrow patient helps clarify proximal tubule dysfunction. *Pediatr Nephrol* **30**, 1027–1031.
- Drueke TB & Massy ZA (2009). Beta2-microglobulin. *Semin Dial* **22**, 378–380.
- Dunn SR, Qi Z, Bottinger EP, Breyer MD & Sharma K (2004). Utility of endogenous creatinine clearance as a measure of renal function in mice. *Kidney Int* **65**, 1959–1967.
- Edwards A, Christensen EI, Unwin RJ & Norden AGW (2021). Predicting the protein composition of human urine in normal and pathological states: quantitative description based on Dent1 disease (*CLCN5* mutation). *J Physiol* **599**, 323–341.
- Eshbach ML & Weisz OA (2017). Receptor-mediated endocytosis in the proximal tubule. *Ann Rev Physiol* **79**, 425–448.
- Gaïde Chevronnay HP, Janssens V, Van Der Smissen P, N'Kuli F, Nevo N, Guiot Y, Levchenko E, Marbaix E, Pierreux CE, Cherqui S, Antignac C & Courttoy PJ (2014). Time course of pathogenic and adaptation mechanisms in cystinotic mouse kidneys. *J Am Soc Nephrol* **25**, 1256–1269.
- Gekle M, Mildenberger S, Freudinger R & Silbernagl S (1995). Endosomal alkalization reduces J_{max} and K_m of albumin receptor-mediated endocytosis in OK cells. *Am J Physiol* **268**, F899–F906.
- Glozzi ML, Espiritu EB, Shipman KE, Rbaibi Y, Long KR, Roy N, Duncan AW, Lazzara MJ, Hukriede NA, Baty CJ & Weisz OA (2020). Effects of proximal tubule shortening on protein excretion in a Lowe syndrome model. *J Am Soc Nephrol* **31**, 67–83.
- Guasch A, Deen WM & Myers BD (1993). Charge selectivity of the glomerular filtration barrier in healthy and nephrotic humans. *J Clin Invest* **92**, 2274–2282.
- Hashimoto S, Adams JW, Bernstein KE & Schnermann J (2005). Micropuncture determination of nephron function in mice without tissue angiotensin-converting enzyme. *Am J Physiol Renal Physiol* **288**, F445–F452.
- Honjo K, Kubagawa Y, Jones DM, Dizon B, Zhu Z, Ohno H, Izui S, Kearney JF & Kubagawa H (2012). Altered Ig levels and antibody responses in mice deficient for the Fc receptor for IgM (*FcμR*). *Proc Natl Acad Sci U S A* **109**, 15882–15887.
- Ichii O, Yabuki A, Ojima T, Matsumoto M & Suzuki S (2006). Rodent renal structure differs among species. *J Vet Med Sci* **68**, 439–445.
- Kalakeche R, Hato T, Rhodes G, Dunn KW, El-Achkar TM, Plotkin Z, Sandoval RM & Dagher PC (2011). Endotoxin uptake by S1 proximal tubular segment causes oxidative stress in the downstream S2 segment. *J Am Soc Nephrol* **22**, 1505–1516.
- Klein-Schneegans AS, Kuntz L, Fonteneau P & Loo F (1989). Serum concentrations of IgM, IgG1, IgG2b, IgG3 and IgA in C57BL/6 mice and their congenics at the *lpr* (lymphoproliferation) locus. *J Autoimmun* **2**, 869–875.
- Kur E, Christa A, Veth KN, Gajera CR, Andrade-Navarro MA, Zhang J, Willer JR, Gregg RG, Abdelilah-Seyfried S, Bachmann S, Link BA, Hammes A & Willnow TE (2011). Loss of *Lrp2* in zebrafish disrupts pronephric tubular clearance but not forebrain development. *Dev Dyn* **240**, 1567–1577.
- Landwehr DM, Schnermann J, Klose RM & Giebisch G (1968). Effect of reduction in filtration rate on renal tubular sodium and water reabsorption. *Am J Physiol* **215**, 687–695.

- Lazzara MJ & Deen WM (2007). Model of albumin reabsorption in the proximal tubule. *Am J Physiol Renal Physiol* **292**, F430–F439.
- Lee JW, Chou CL & Knepper MA (2015). Deep sequencing in microdissected renal tubules identifies nephron segment-specific transcriptomes. *J Am Soc Nephrol* **26**, 2669–2677.
- Leheste JR, Rolinski B, Vorum H, Hilpert J, Nykjaer A, Jacobsen C, Aucouturier P, Moskaug JO, Otto A, Christensen EI & Willnow TE (1999). Megalin knockout mice as an animal model of low molecular weight proteinuria. *Am J Pathol* **155**, 1361–1370.
- Letts RF, Zhai XY, Bhikha C, Grann BL, Blom NB, Thomsen JS, Rubin DM, Christensen EI & Andreasen A (2017). Nephron morphometry in mice and rats using tomographic microscopy. *Am J Physiol Renal Physiol* **312**, F210–F229.
- Limbutara K, Chou C-L & Knepper MA (2020). Quantitative proteomics of all 14 renal tubule segments in rat. *J Am Soc Nephrol* **31**, 1255–1266.
- Liu D, Wen Y, Tang TT, Lv LL, Tang RN, Liu H, Ma KL, Crowley SD & Liu BC (2015). Megalin/cubulin-lysosome-mediated albumin reabsorption is involved in the tubular cell activation of NLRP3 inflammasome and tubulointerstitial inflammation. *J Biol Chem* **290**, 18018–18028.
- Long KR, Rbaibi Y, Bondi CD, Ford BR, Poholek AC, Boyd-Shiarski CR, Tan RJ, Locker JD & Weisz OA (2022). Cubilin-, Megalin- and Dab2-dependent transcription revealed by CRISPR/Cas9 knockout in kidney proximal tubule cells. *Am J Physiol Renal Physiol* **322**, F14–F26.
- Long KR, Shipman KE, Rbaibi Y, Menshikova EV, Ritov VB, Eshbach ML, Jiang Y, Jackson EK, Baty CJ & Weisz OA (2017). Proximal tubule apical endocytosis is modulated by fluid shear stress via an mTOR-dependent pathway. *Mol Biol Cell* **28**, 2508–2517.
- Ma J, Guan M, Bowden DW, Ng MC, Hicks PJ, Lea JP, Ma L, Gao C, Palmer ND & Freedman BI (2016). Association analysis of the *cubilin* (*CUBN*) and *megalin* (*LRP2*) genes with ESRD in African Americans. *Clin J Am Soc Nephrol* **11**, 1034–1043.
- Martins JR, Haenni D, Bugarski M, Polesel M, Schuh C & Hall AM (2021). Intravital kidney microscopy: entering a new era. *Kidney Int* **100**, 527–535.
- Meneton P, Ichikawa I, Inagami T & Schnermann J (2000). Renal physiology of the mouse. *Am J Physiol Renal Physiol* **278**, F339–F351. <https://doi.org/10.1152/ajprenal.2000.278.3.F339>
- Mink JG & Benner R (1979). Serum and secretory immunoglobulin levels in preleukaemic AKR mice and three other mouse strains. *Adv Exp Med Biol* **114**, 605–612.
- Mori KP, Yokoi H, Kasahara M, Imamaki H, Ishii A, Kuwabara T, Koga K, Kato Y, Toda N, Ohno S, Kuwahara K, Endo T, Nakao K, Yanagita M, Mukoyama M & Mori K (2017). Increase of total nephron albumin filtration and reabsorption in diabetic nephropathy. *J Am Soc Nephrol* **28**, 278.
- Nagai J, Christensen EI, Morris SM, Willnow TE, Cooper JA & Nielsen R (2005). Mutually dependent localization of megalin and Dab2 in the renal proximal tubule. *Am J Physiol Renal Physiol* **289**, F569–F576.
- Nagai J, Sato K, Yumoto R & Takano M (2011). Megalin/cubilin-mediated uptake of FITC-labeled IgG by OK kidney epithelial cells. *Drug Metab Pharmacokinet* **26**, 474–485.
- Norden AG, Lapsley M, Lee PJ, Pusey CD, Scheinman SJ, Tam FW, Thakker RV, Unwin RJ & Wrong O (2001). Glomerular protein sieving and implications for renal failure in Fanconi syndrome. *Kidney Int* **60**, 1885–1892.
- Park CH & Maack T (1984). Albumin absorption and catabolism by isolated perfused proximal convoluted tubules of the rabbit. *J Clin Invest* **73**, 767–777.
- Park HJ, Fan Z, Bai Y, Ren Q, Rbaibi Y, Long KR, Gliozzi ML, Rittenhouse N, Locker JD, Poholek AC & Weisz OA (2020). Transcriptional programs driving shear stress-induced differentiation of kidney proximal tubule cells in culture. *Front Physiol* **11**, 587358.
- Peti-Peterdi J, Kidokoro K & Riquier-Brison A (2015). Novel in vivo techniques to visualize kidney anatomy and function. *Kidney Int* **88**, 44–51.
- Raghavan V, Rbaibi Y, Pastor-Soler NM, Carattino MD & Weisz OA (2014). Shear stress-dependent regulation of apical endocytosis in renal proximal tubule cells mediated by primary cilia. *Proc Natl Acad Sci U S A* **111**, 8506–8511.
- Ren Q, Weyer K, Rbaibi Y, Long KR, Tan RJ, Nielsen R, Christensen EI, Baty CJ, Kashlan OB & Weisz OA (2020). Distinct functions of megalin and cubilin receptors in recovery of normal and nephrotic levels of filtered albumin. *Am J Physiol Renal Physiol* **318**, F1284–F1294.
- Schuh CD, Polesel M, Platonova E, Haenni D, Gassama A, Tokonami N, Ghazi S, Bugarski M, Devuyt O, Ziegler U & Hall AM (2018). Combined structural and functional imaging of the kidney reveals major axial differences in proximal tubule endocytosis. *J Am Soc Nephrol* **29**, 2696–2712.
- Weinstein AM, Weinbaum S, Duan Y, Du Z, Yan Q & Wang T (2007). Flow-dependent transport in a mathematical model of rat proximal tubule. *Am J Physiol Renal Physiol* **292**, F1164–F1181.
- Weisz OA (2021). Endocytic adaptation to functional demand by the kidney proximal tubule. *J Physiol* **599**, 3437–3446.
- Weisz OA & Baty CJ (2018). Lemmings into the sea or back across the bridge? The fate of albumin in nephrotic syndrome. *Kidney Int* **93**, 296–298.
- Weyer K, Andersen PK, Schmidt K, Mollet G, Antignac C, Birn H, Nielsen R & Christensen EI (2018). Abolishment of proximal tubule albumin endocytosis does not affect plasma albumin during nephrotic syndrome in mice. *Kidney Int* **93**, 335–342.
- Weyer K, Storm T, Shan J, Vainio S, Kozyraki R, Verroust PJ, Christensen EI & Nielsen R (2011). Mouse model of proximal tubule endocytic dysfunction. *Nephrol Dial Transplant* **26**, 3446–3451.
- Woodhall PB, Tisher CC, Simonton CA & Robinson RR (1978). Relationship between para-aminohippurate secretion and cellular morphology in rabbit proximal tubules. *J Clin Invest* **61**, 1320–1329.
- Zhai XY, Birn H, Jensen KB, Thomsen JS, Andreasen A & Christensen EI (2003). Digital three-dimensional reconstruction and ultrastructure of the mouse proximal tubule. *J Am Soc Nephrol* **14**, 611–619.

Zhai XY, Nielsen R, Birn H, Drumm K, Mildenerberger S, Freudinger R, Moestrup SK, Verroust PJ, Christensen EI & Gekle M (2000). Cubilin- and megalin-mediated uptake of albumin in cultured proximal tubule cells of opossum kidney. *Kidney Int* **58**, 1523–1533.

Additional information

Data availability statement

The authors confirm that the data supporting the findings of this study are available within the article and its supplementary materials.

Competing interests

The authors report no conflict of interest in connection with this article.

Author contributions

A.E., C.J.B., K.E.S. and O.A.W. designed research. A.E., K.R.L., C.J.B. and K.E.S. performed research. A.E., C.J.B., K.E.S. and O.A.W. analysed data. A.E. and O.A.W. wrote the paper. All authors revised the paper and approved the final version of the manuscript. All authors agree to be accountable for all aspects of the work in ensuring that questions related to the accuracy or

integrity of any part of the work are appropriately investigated and resolved. All persons designated as authors qualify for authorship, and all those who qualify for authorship are listed.

Funding

This work was funded by National Institutes of Health grants R01-DK118726 (O.A.W.), R01-DK125049 (O.A.W.), S10-OD021627 (O.A.W.), F31DK121394 (K.E.S.) and the Pittsburgh Center for Kidney Research (P30 DK079307).

Acknowledgements

The authors thank Dr Ossama Kashlan for helpful discussions.

Keywords

cubilin, endocytosis, kidney, megalin, proteinuria

Supporting information

Additional supporting information can be found online in the Supporting Information section at the end of the HTML view of the article. Supporting information files available:

Peer Review History

Statistical Summary Document